

A Review of Shape Memory Polymers and Composites: Mechanisms, Materials, and Applications

Yuliang Xia, Yang He, Fenghua Zhang, Yanju Liu,* and Jinsong Leng*

Over the past decades, interest in shape memory polymers (SMPs) has persisted, and immense efforts have been dedicated to developing SMPs and their multifunctional composites. As a class of stimuli-responsive polymers, SMPs can return to their initial shape from a programmed temporary shape under external stimuli, such as light, heat, magnetism, and electricity. The introduction of functional materials and nanostructures results in shape memory polymer composites (SMPCs) with large recoverable deformation, enhanced mechanical properties, and controllable remote actuation. Because of these unique features, SMPCs have a broad application prospect in many fields covering aerospace engineering, biomedical devices, flexible electronics, soft robotics, shape memory arrays, and 4D printing. Herein, a comprehensive analysis of the shape recovery mechanisms, multifunctionality, applications, and recent advances in SMPs and SMPCs is presented. Specifically, the combination of functional, reversible, multiple, and controllable shape recovery processes is discussed. Further, established products from such materials are highlighted. Finally, potential directions for the future advancement of SMPs are proposed.

temperature (T_{trans}), and retains the deformed shape after cooling down. They revert from the deformed shape to the permanent shape by reheating. The shape memory effect has been found in a variety of polymers including amorphous polymer,^[6,7] semicrystalline polymer,^[8,9] and liquid crystalline elastomer (LCE).^[10] After years of research, people have obtained a preliminary understanding of shape memory effect based on the development of thermomechanical theory, especially the thermoviscoelastic theory and phase transition theory, which can provide physical interpretation. In addition, clarifying the crosslinked chemical structure is seminal for improving the polymer performance and exploring novel shape memory behavior.

At present, there have been many studies on one-way, two-way, and multiple SMPs. One-way shape memory effect has been found in conventional crosslinked

1. Introduction


Stimuli-responsive materials are regarded as smart because they can sense their surroundings and produce direct and straightforward responses.^[1] The research of stimuli-responsive materials was inspired by the bionic behavior of organisms. For example, the Venus flytrap can close the leaf rapidly to capture animals passing by within 100 ms when its trigger hairs feel the physical stimulation.^[2] As polymeric stimuli-responsive materials, shape memory polymers (SMPs) have provoked interest from scientists since the 1960s. It was revealed that γ -ray irradiated polyethylene (PE) could show memory effect under low-high temperature cycles.^[3–5] SMPs present a permanent shape at room temperature, deforms at a high transition

polymers.^[11] Thus, one-way SMPs have been extended to commercial applications for quite a long time as one of the most common smart materials. Examples include heat-shrinkable tubes, heat-shrinkable labels, and heat-shrinkable toys.^[12] In the high-tech area, one-way self-deployable hinges^[13] and smart surgery devices^[14] were developed. Two-way SMPs, also called reversible SMPs, refer to polymers that autonomously deform at high temperatures and revert at low temperatures between two desired shapes. The mechanism of two-way shape memory effect involves the directional rearrangement of the molecular chain as temperature changes, and it has been utilized in the preparation of a number of LCEs^[10] and semicrystalline polymers.^[8,9] The development of two-way SMPs with good mechanical properties and good shape memory performance is possible to replace the shape memory alloy in the future. Moreover, the polymers capable of memorizing more than one temporary shape are defined as multiple SMPs, which can be referred to as the copolymer of a set of one-way SMPs with diverse T_{trans} .^[15] The multiple shape memory effect allows the polymer to switch into a set of shapes through the relevant programming process. A profound understanding of these shape memory phenomena could bring novel application opportunities with advanced properties.

Herein, we summarize the significant advancements of SMPs systematically. We start with some basic concepts to interpret the definition of shape memory effect, followed by the state-of-art progress in different shape memory mechanisms

Y. Xia, Dr. Y. He, Dr. F. Zhang, Prof. J. Leng
Center for Composite Materials and Structures
Harbin Institute of Technology (HIT)
Harbin 150080, P. R. China
E-mail: lengjs@hit.edu.cn

Prof. Y. Liu
Department of Astronautical Science and Mechanics
Harbin Institute of Technology (HIT)
Harbin 150001, P. R. China
E-mail: yj_liu@hit.edu.cn

 The ORCID identification number(s) for the author(s) of this article can be found under <https://doi.org/10.1002/adma.202000713>.

DOI: 10.1002/adma.202000713

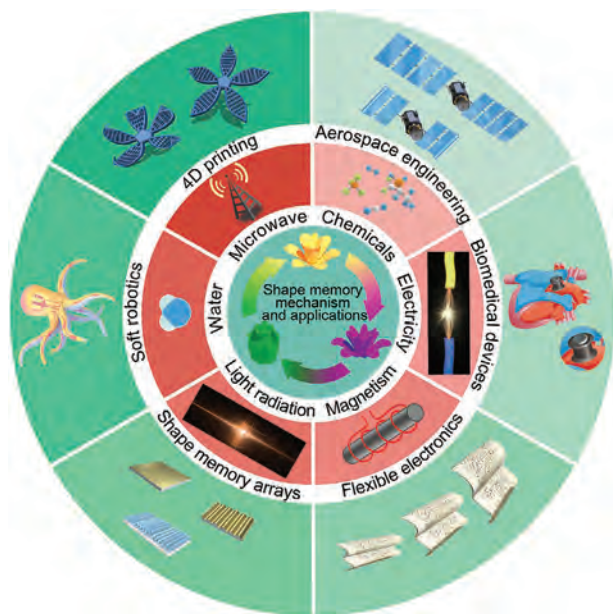


Figure 1. Scheme of the shape memory polymers (SMPs): mechanism, actuation methods, and applications.

and approaches to the design of SMPs. Insights into the kinetics of the molecular chain are essential for understanding the phase transition process and overall regulating the shape memory behavior. Thus, the polymer model, chemical structure, and synthesis strategies presented here would be of great value. Meanwhile, the strategies to construct shape-memory polymer composites (SMPCs) with improved performance and controllable activating capability are illustrated. The shape memory actuation methods, including electricity,^[16] magnetic field,^[17] light,^[18] and water,^[19] are presented. Recent progress in shape memory applications is highlighted (Figure 1). Last, future prospects and challenges in designing novel SMPs are also discussed. We hope to gain further insights into the evolution of shape memory polymeric materials. The structure of this review is organized in the following order: introduction of SMPs; shape memory mechanism and characterization; one-way, two-way, and multiple SMPs; multifunctional SMPCs, and their applications.

2. General Aspects of SMPs

2.1. Definition of SMPs

It is necessary to determine if the shape programming process is required to identify a polymer as an SMP. Shape memory programming is the first step in a shape memory cycle to determine the polymer transforming pathway. The programming process of SMPs involves shape deforming, shape fixing, and evacuation of the external stress. Before the programming process, the polymers need to be deformed under external stress accompanied by heating. A high temperature can increase the entropy of the polymer, decrease the energy barrier, and make the molecular chain easy to move, which makes the polymer more comfortable to manipulate. After the polymer is deformed into a desired temporary shape, it will be fixed with



Yuliang Xia received his B.S. degree in materials chemistry in 2019 from Harbin Institute of Technology. He is currently a Ph.D. candidate under the supervision of Prof. Jinsong Leng at Harbin Institute of Technology. His research focuses on the synthesis and optimization of shape memory intelligent materials, as well as exploring their underlying mechanism and applications.



Yanju Liu is a full professor in the Department of Aerospace Science and Mechanics at the Harbin Institute of Technology (HIT), China. She obtained her Ph.D. degree in material science from HIT, China in 1999. Her research interests are in the field of smart materials and structures, including stimuli-responsive materials, such as ER/MR fluids, electroactive polymers, shape memory polymers, and their composites.



Jinsong Leng is a Cheung Kong Chair Professor at Harbin Institute of Technology. He received his B.S. and Ph.D. in engineering mechanics and composite materials from HIT in 1990 and 1996, respectively. His research interests cover shape memory polymers and composites, 4D printing, sensors and actuators, structural health monitoring, and multifunctional nanocomposites.

the decreasing temperature and maintained by external stress. The conditions include physical and chemical changes that can block the movement of polymer molecular chains. Finally, the temporary shape can be obtained after cooling down and will not alter as the external stress is withdrawn.

The temporary shape can be retained for a long time without an external stimulus. The stress and energy are stored in the polymer during the programming process with the increasing entropy. Hence, the temporary shape is more unstable than the original shape. When the material is exposed to a suitable external stimulation, the internal stress and energy will be released, causing the molecular chain to possess mobility

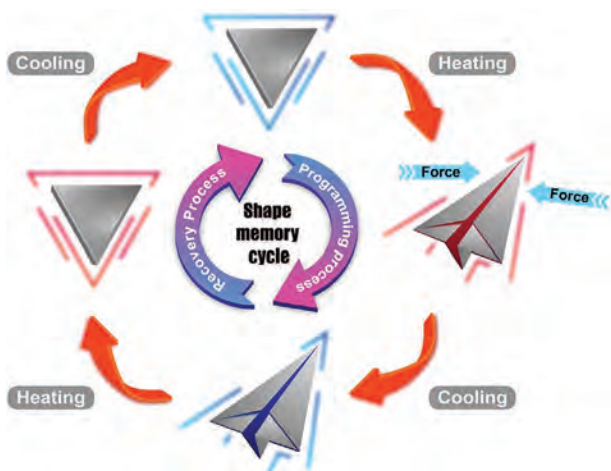


Figure 2. Scheme of shape memory cycle.

again. The polymer then returns to the original shape after the stimulation^[20] (Figure 2). The programming process can be repeated multiple times; therefore, SMPs can possess different temporary shapes but only one permanent shape.

The programming process is not dependent on the material synthesis but can be recognized as posttreatment to define the material's shape recovery path. If a polymer can alter its shape under specific stimulus without the shape programming process, it is a shape-changing polymer rather than an SMP. For example, most hydrogels that consist of poly(*n*-isopropylacrylamide) (PNIPA) can swell and deswell in water under temperature changes. The changing shape of PNIPA hydrogel is caused by various degrees of shrinkage of the molecular chain at different temperatures resulting in the ingress and egress of water molecules. This process requires the physical nature of PNIPA hydrogel rather than shape programming; thus, these hydrogels cannot be defined as SMPs. With the precise definition of shape memory programming, it is advisable to classify the programmable polymers as SMPs.

2.2. Thermomechanical Theory of SMPs

It is necessary to analyze the structure of SMPs from a microscopic perspective to elucidate the cause of the shape memory effect. The thermoviscoelastic theory model is used to explain the thermodynamic behavior in SMPs. The molecular chain can be considered as a small spring. These springs are tiny in diameter and large in length, and they entangle with each other when being mixed. In the SMPs, the polymer has higher entropy because of the random arrangement of the springs at room temperature. When the temperature rises, the molecular mobility will increase, and the polymer produces thermoviscoelasticity. At this time, the springs can be stretched and oriented by an external force, and the alignment can cause decreased entropy of the polymer. If the temperature decreases without changing the external force, then the polymer loses thermoviscoelasticity, the molecular motion is weakened, and the springs cannot return to their original form in this case. During this process, the stress is stored in the springs in the form of elastic potential energy.

When the temperature rises again, the springs gain thermoviscoelasticity and the stored elastic potential energy is released.

It is noteworthy that the friction between the springs generates heat, consuming the elastic potential energy that should be stored inside the springs and causing irreversible viscosity deformation. The viscosity change is considered as the compressing and expanding process of a dashpot. By involving the dashpot concept into the thermoviscoelastic theory, we can build a standard linear solid (SLS) model to design SMPs elements.^[21–23] Throughout the process, the elasticity stores the work done by the external force, and the viscosity consumes the work done by the external force. Therefore, it is necessary to ensure that no excessive slippage exists between the springs, which leads to the macroscopic deformation without entropic change. In 1994, Buckley et al.^[24] demonstrated a 3D glass-rubber constitutive model to explain the features of amorphous SMPs near the glass transition temperature (T_g). This model illustrated the stress–strain relationship of thermoviscoelastic deformation and the problem of conformational entropy function. Moreover, Tobushi et al.^[25] established a four-element model to explain the irreversible deformation generated by the relative friction between SMPs molecules. The four-element model involved the elastic modulus, viscosity, retardation time, and slip element. The thermoviscoelastic theory can clearly explain the mechanical behavior of SMPs, but there are still some shortcomings in the storage and release of enthalpy energy.

The phase transition theory is more suitable for explaining the shape transition behavior of SMPs from the thermomechanical perspective.^[26–28] The phase composition of SMPs can be divided into two parts (i.e., the frozen and the active phases). The frozen phase (hard phase) occurs when the enthalpy energy changes inside the material and the molecular chain is stretched or rotated to ensure that the internal structure does not change. Any further conformational motion of the content is impossible in the frozen phase. By contrast, the active phase (soft phase) consists of dynamic bonds. In the active phase, deformation is possible, and the molecules can rotate, elongate, and compress. The frozen phase is the primary phase in the glass state. As the polymer transforms from the glass state to the rubbery state, parts of the frozen phase transform into the active phase, and the ratio of the frozen phase to the active phase changes. During the programming process, the conformational movements are stored in the active phase. As the temperature decreases, the active phase transforms into the frozen phase with the stress localized. Stress at this time is not enough to generate adequate enthalpy to drive the shape recovery process. When the temperature rises, the frozen phase turns into an active phase and the stored stress is released. The transformations of the frozen and active phases embody the glass transition behavior in the thermodynamic cycle and explain the storage and release process of stress in the shape memory process. Based on the phase transition theory, Yu et al.^[29] confirmed the impact of that programming process on the shape recovery behavior. The shape recovery speed is strongly dependent on the programming and recovery temperatures. During the loss of modulus in the de-frozen process, the driving force reduces as a result of the slow recovery process. The phase transition theory supports the establishment of most thermodynamic models at the macromolecular scale.

The thermoviscoelastic and phase transition theories have certain complementarity. The two theoretical models can be combined to establish a more accurate and reasonable constitutive model to study more complicated SMPs structures accurately.^[30,31] Qi et al.^[32] investigated the finite deformation and thermo-mechanical behaviors of thermally induced SMPs. A 3D constitutive model was developed based on the experimental observation of SMPs to describe the thermo-mechanic response of SMPs. The model established on the stress-strain experiment captured the shape recovery behavior of SMPs well. However, it did not fully achieve the stress recovery, but accounted for the impact of the temperature rate on the thermo-mechanic behavior of SMPs. Leng et al.^[33] combined the thermoviscoelastic and phase transition theories into a general model equation. This model could explain the mechanism of multishape memory effect and phase transition behavior. Mechanical, storage, and thermal expansion strains were vital factors in the model. Recently, Lu et al.^[34,35] used internal stress as a function to model the phase transition behavior so as to get a better understanding of the shape memory effect at a macromolecular scale. In the study, the shape memory effect under complex stress was studied based on the influence of polymer temperature on shape memory effect. The frozen volume model was established to characterize the macromolecular structure and shape memory effect of amorphous SMPs. The results demonstrated an excellent agreement between the theoretical and experimental results. The developed constitutive models are effective in studying the thermomechanical behavior of SMPs and predicting the shape memory behavior.

2.3. Mechanism and Classification of One-Way SMPs

According to the macromolecular view, one-way SMPs have two structures. The switchable segments affix the temporary shape during shape programming, and the netpoints define the permanent shape.^[36] The switchable segments can lock the energy to make sure that it cannot be released without a specific stimulation. When the material is heated and subject to an external force, the deformation of the material as a whole will be caused by the changes in tensile or compression of the switchable segments. The part used to connect these switchable segments is called netpoints. These netpoints can be chemically crosslinking points, which are the central atoms of the polymer crosslinked networks; or it can also physically be a fragment, such as microscopic phases and domains.

2.3.1. One-Way SMPs Based on Phase Transition

Conventional SMPs typically consist of polymer chains with varying motion states across T_{trans} . The softening and hardening of the transition phase in the polymer enable the lock and unlock of the temporary shape.^[37] This process requires direct or indirect heating to change phase activity and ensure enough enthalpy for shape changes. The most primitive one-way SMPs stem from the amorphous phase transition behavior.^[38] The amorphous phase occupies a specific part of the polymer, which decides the T_g region. When the temperature reaches T_g ,

the polymer gains better ductility and deformability than that at normal temperature. At this point, the polymer transforms from the glassy state to the rubbery state. The molecular chain becomes flexible enough to be stretched, coiled, or bent under the external stress, leading the deformation of the polymer. The T_g range can be broad or narrow, depending on the difference in the molecular chain structure.

In terms of the crystalline and semicrystalline polymers, the melting temperature (T_m) is the crucial factor for triggering the shape memory behavior.^[39] This phenomenon is common in blends of crystalline polymers with other polymers without shape memory effect or block copolymers. The crystalline polymers act as a soft region in the blend, whereas the polymers without shape memory effect act as a rigid region. When heated across the T_m , the crystalline part softens to make the blend polymer easy to manipulate. The polymer without shape memory effect has a higher T_m compared to the crystalline polymer, which enables the blended polymer to maintain a certain solid shape. Currently, one-way SMPs based on phase transition are the most advantageous because of the relatively simple mechanism and mature production. Through the introduction of different reinforcement materials to the polymer matrix, multifunctional shape memory composites were developed with high mechanical performance and remote shape memory actuation capability. (Section 3) The relevant applications will be demonstrated in Section 4

2.3.2. One-Way SMPs Based on Reversible Switches

Besides the thermal phase-controlled shape memory effect, various nonthermal approaches have been devised to determine whether the nonthermal strategies can trigger the shape memory process. Most of these methods focus on the reversible covalent and noncovalent bonds. In 2005, Lendlein et al.^[40] demonstrated that the incorporation of the photosensitive units in the polymer could produce the shape memory effect. Photoreversible [2 + 2] cycloaddition groups, which are cinnamic acid and cinnamylidene acetic acid, were grafted onto the permanent polymer network. The photo-reversible reaction was triggered by the alternation of the exposing wavelengths. The polymer deformed into a temporary shape with UV light irradiation at $\lambda > 260$ nm and returned to the permanent shape at $\lambda < 260$ nm. Compared to the thermally triggered SMPs, these polymers were stable under 50 °C, but take a long time for shape fixing and recovery (about 1.5 h per procedure), showing a low fix ratio (R_f). Moreover, Wu et al.^[41] incorporated the cinnamamide moieties in the multi-block polyester urethanes to realize the one-way shape memory effect (Figure 3a). The shape recovery capability based on photo reversible covalent bond has been studied further.^[42–44]

Different from the light-triggered photo reversible reaction, the light-induced isomerization is another mechanism that can replace the thermal phase transition behavior in the polymer. Lee et al.^[45] introduced this phenomenon to SMPs. Azobenzene molecules were grafted on a series of polymer networks including liquid crystalline network, polyimide, and other functional units.^[46] The deformed shape was fixed and recovered with blue-green light irradiation ($\lambda = 442$ nm), which induced the *trans-cis-trans* reorientation of azobenzene

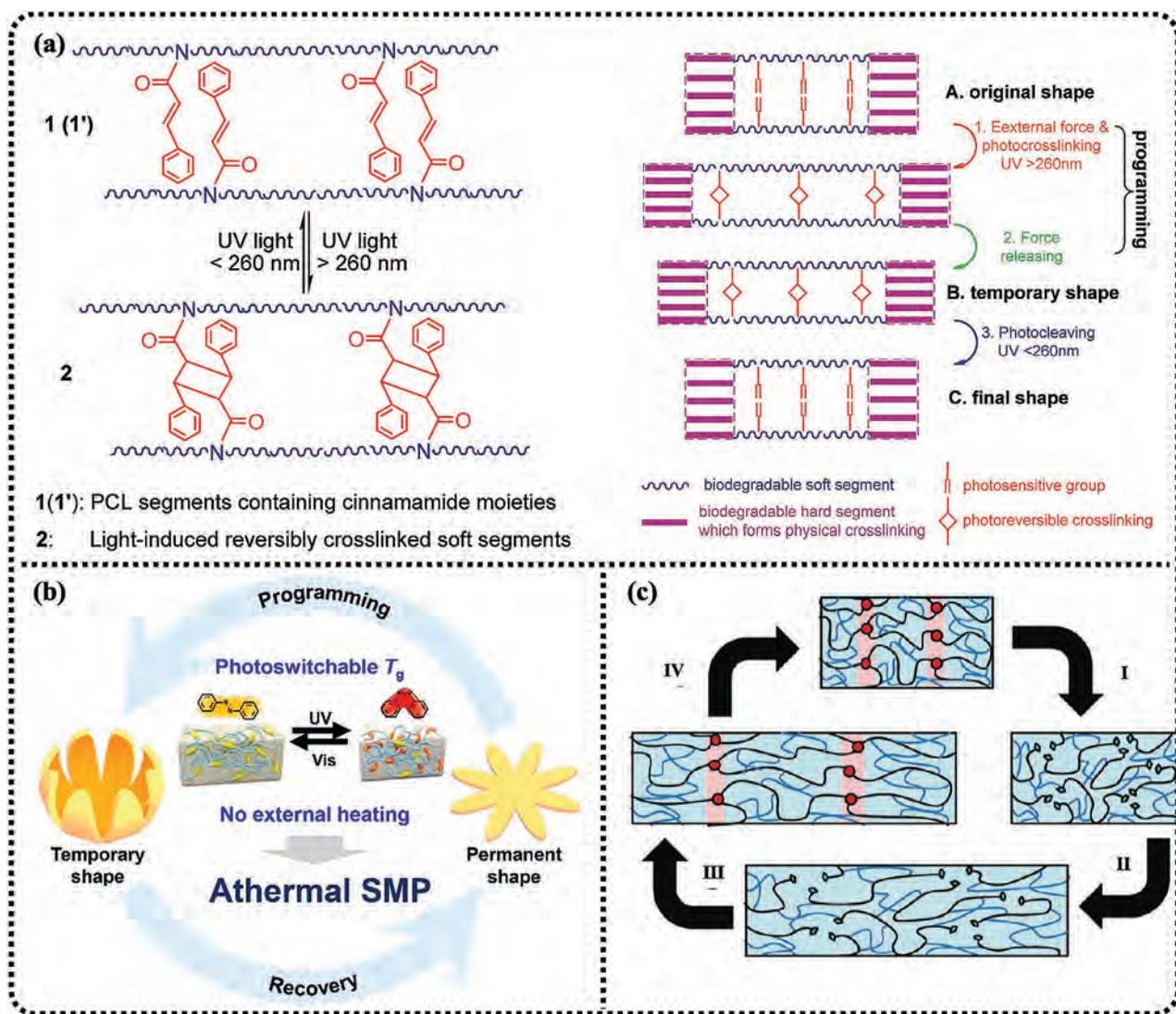


Figure 3. a) Light-induced [2 + 2] cycloaddition reaction (left) and shape memory effect (right) of photoresponsive multiblock polyester urethane. Reproduced with permission.^[41] Copyright 2011, American Chemical Society. b) Athermal shape memory effect induced by reversible *trans*–*cis* isomerization. Reproduced with permission.^[47] Copyright 2019, American Chemical Society. c) Shape memory effect with metal–ligand complexes triggered by UV light. Reproduced with permission.^[49] Copyright 2011, American Chemical Society.

chromophores. The blue-green light was eye-safe and could trigger the isomerization reaction rapidly ($\ll 5$ min).^[18] Zhang et al.^[47] reported a thermal polymer containing azobenzene unit to demonstrate the shape memory behavior at room temperature. Instead of irradiation heating, the T_g is photo-switchable and corresponds to the UV and visible light irradiations (Figure 3b). Therefore, the light-triggered molecular switches can substitute the thermo-activated phase transition. However, the photoresponsive reaction needs the deep penetration of the light into the polymer with a particular transmittance. Thus, these light-induced methods are not effective in bulk SMPs.

Thermo-induced covalent bond exchange reaction is another example. Here, the enthalpy triggers the reversible chemical reaction between the molecule chains. Various reversible chemical reactions can be used to trigger the shape memory behavior. Disulfide bond as a reversible chemical unit can exhibit shape

memory effect during the redox reaction. Nishio et al.^[48] introduced the thiol units to the cellulose acetate backbones. The shape memory behavior was triggered in the dimethyl sulfoxide (DMSO) solutions through the change of the redox state of mercapto groups. It took 96 h at 30 °C to recover the permanent shape. The shape memory behavior has been observed in polymers with reversible physical interactions as well. These physical interactions include strong hydrogen bonding, typically involve ureidopyrimidinone molecules and metal–ligand coordination bonds^[49] (Figure 3c). In comparison with the covalent bond, the macromolecular interactions ensure the reproducibility of polymers because the noncovalent bonds can be separated when external stress exceeds the limit and they can re-join upon heating.

The molecules' bond reversibility is an essential factor in producing shape memory effect compared to the nonreversible chemical reaction. Rowan et al.^[50] improved the shape memory effect

based on the polymer with the disulfide bond. They synthesized the polydisulfide network by crosslinking the 1,6-hexanedithiol, 1,5-hexadiene, and the tetrathiol. The targeted semicrystalline network demonstrated shape memory features below 80 °C, and the photo-healable property under UV light curing. The permanent shape was also reprogrammable at relatively high temperatures (≥ 180 °C). The transesterification is another example. Polymers with ester group showed shape memory effect at low temperature and self-healing capability at high temperature as well.^[51,52] Compared with the disulfide exchange reaction, both of them demonstrated nonreversible molecule switches upon heating. However, the shape memory effect demonstrated by these polymers is not based on the chemical reaction. When the covalent bond captures enough energy, the exchange reaction happens, and the polymer network is reset into a new permanent shape. Hence, the shape memory effect should be attributed to thermomechanical behavior. Based on the nonreversible exchange reaction, the transesterification reaction and disulfide exchange reaction introduce the self-healing functionality and recyclability into the material. The shape recovery phenomenon based on the covalent bond is akin to noncovalent bonds. Whether a more general shape memory theory can be established is a question that needs to be answered by further studies.

2.4. Two-Way SMPs Mechanism and Classification

One-way SMPs exhibit an irreversible shape recovery by shifting from the temporal to the permanent shape in one shape memory cycle. Differently, two-way SMPs exhibit a reversible shape-changing process between the initial and temporary shapes during the cycle. For this reason, two-way SMPs have received more attention compared to one-way SMPs based on their ability to change shapes in response to external stimuli. Studies on two major categories of two-way SMPs, the semicrystalline polymer and LCE, are reviewed next. Both comprise a chemical structure that can transform the molecular anisotropy under desired temperatures.

2.4.1. Two-Way SMPs Based on the Semicrystalline Polymer

Mather et al.^[8] in 2008 demonstrated that a semicrystalline polymer network exhibited a reversible shape memory property under constant stress. Poly(cyclooctene) with different crosslinking degrees was synthesized in the study. The semicrystalline network with a constant tensile load elongated when cooled across the T_m , and contracted when heated. The result of the dynamic mechanical analysis revealed that the crystalline elongation during cooling and the melting contraction upon heating were responsible for the two-way shape memory property. The crystal structure changed the strain according to the tensile direction of the stress. A constitutive model was subsequently developed to quantitatively capture the two-way shape memory effect in the semicrystalline polymer, in which the stretch-induced crystallization was found with a decrease in temperature.^[53] Different studies on this one-dimensional constitutive model have shown consistent results.

The two-way shape memory effect can be brought about by external stress along one axis, which leads to the anisotropy

of the molecules during the heating and cooling process. Koerner et al.^[54] incorporated the carbon nanotube (CNT) into the thermoplastic polymer. The CNT absorbed the infrared light for remote control of shape recovery behavior. As the polymer deformed in response to external stress, the CNT got aligned in the direction of the force. The alignment of the CNT affected the polymer crystallite distribution, impacted the shape stability, and changed the recovered permanent shape. This phenomenon provides an excellent idea for the synthesis of two-way SMPs through the introduction of a second material into the polymer network to control polymer crystal distribution. Lendlein et al.^[55] synthesized two-way SMPs that exhibited the reversible bidirectional shape memory effect without any external stress. The polymer contained two segments: poly(ω -pentadecalactone) (PPD) segments with a higher T_{trans} of about 64 °C and poly(ϵ -caprolactone) (PCL) segments with a lower T_{trans} of about 34 °C. The PPD segments served as geometry-determining domains, whereas the PCL functioned as the actuator domain. During the programming process, the polymer was heated above the $T_{trans,high}$ under external stress, thus being deformed into a temporary shape. When the temperature was reduced below the $T_{trans,low}$, the temporary shape was fixed. This process was similar to programming process of the one-way SMPs. However, during the process, the shape of the PPD geometry-determining domain was altered. The temperature changed between $T_{trans,low}$ and $T_{trans,high}$, causing anisotropy changes in the PCL region along the PPD direction without the application of external stress; hence, a two-way shape memory effect was generated. Remarkably, the temporary shape could be reshaped when the polymer was heated above the $T_{trans,high}$ due to the transition of the PPD segments. This constituted the first two-way SMP based on intrinsic stress direction with a strict definition. A single crosslinked polyurethane (PU) network with C–ON bond was later incorporated with a synchronous bond fission/radical recombination behavior of C–ON bonds that caused internal tensional force.^[56] The polymer demonstrated a two-way shape memory effect upon 60 °C with great recovery stress. Various reversible networks of semicrystalline polymers have been reported accordingly.^[57–60] Meng et al.^[57] demonstrated the two-way shape memory effect of semicrystalline PCL (Figure 4a). Gao et al.^[58] reported the reversible shape memory effect based on polyolefin elastomers (Figure 4b). Zhou et al.^[59] presented a general strategy for generating a two-way shape memory effect in semicrystalline polymers (Figure 4c). Additionally, other methods involving SMPs bilayer structures that demonstrate a two-way shape memory effect have also been reported.^[61]

2.4.2. Two-Way SMPs Based on LCE

The LCE constitutes another category of two-way SMPs. Classical liquid crystal (also called mesogen), which is typically fluid with relatively stiff rod molecules, consists of two benzene rings linked with an unrotatable function group. Cooling the liquid crystal across the clearing point (T_c) will turn the molecular arrangement from the isotropy to anisotropy state, resulting in the optical birefringence and phase transition. This is a unique characteristic of the liquid crystal, which is caused by the nonrotatability of the rigid rod molecules. The liquid crystal monomers

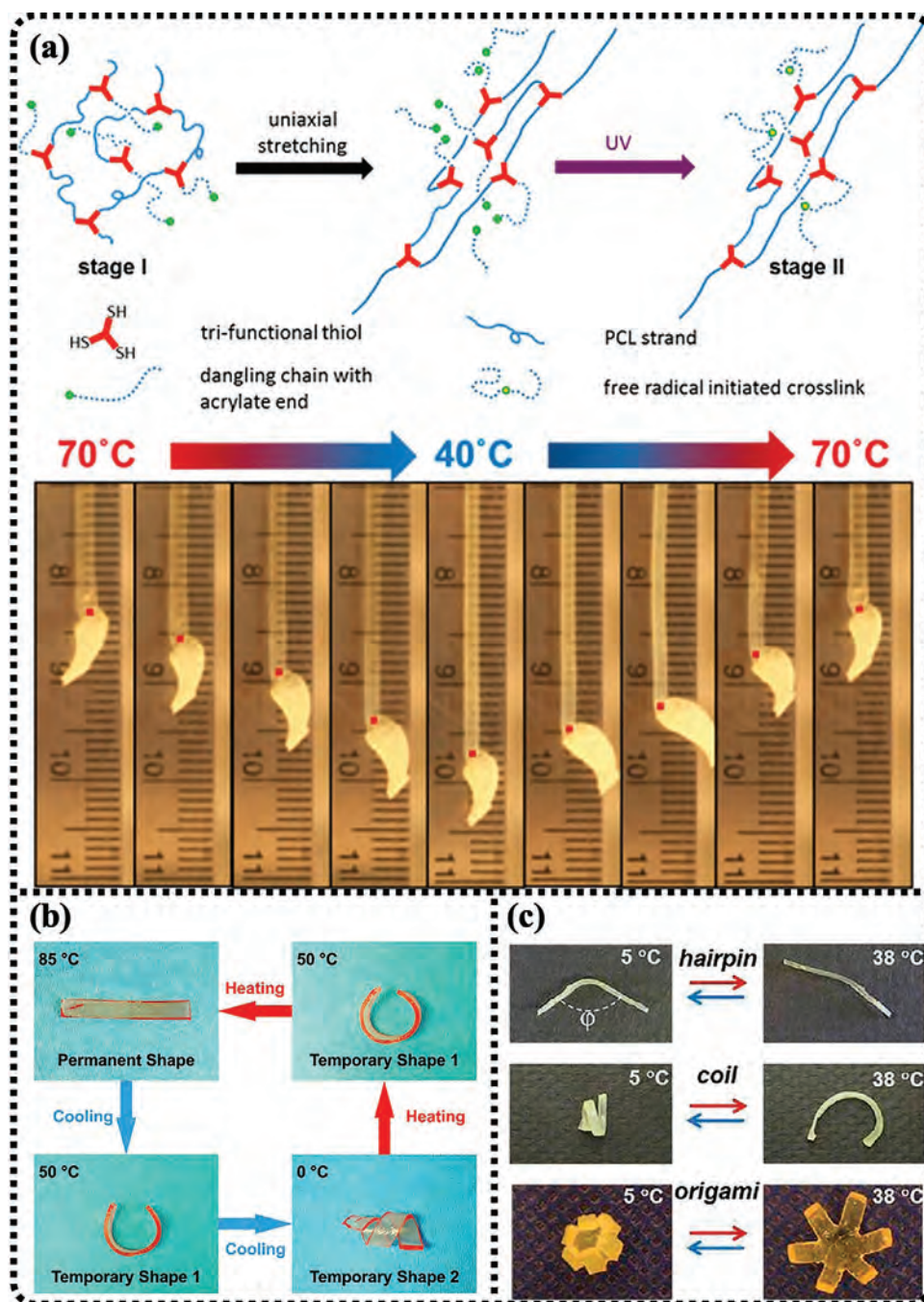


Figure 4. a) Preparation of dual-cure network, stress-free actuators, and reversible actuation behavior. Reproduced with permission.^[57] Copyright 2014, American Chemical Society. b) Reversible shape memory effect of polyolefin thermoplastic elastomer. Reproduced with permission.^[58] Copyright 2019, American Chemical Society. c) Reversible shape transition of crosslinked poly(octylene adipate). Reproduced with permission.^[59] Copyright 2014, American Chemical Society.

contain a stiff core mesogenic group with the functional group connected through the flexible spacers, which follow the basic rules of the liquid crystal. And the LCE is obtained through the chemical crosslinking of the liquid crystal monomers. Finkelmann et al.^[62] successfully synthesized the LCE by linking the siloxanes group with the mesogenic group. The mesogenic domain aligned along one axis with the magnetic field, stretching force, or the other applied field. Heating the LCE above the T_c

will change the anisotropy state of the polymer chain leading to the contraction of the sample. In contrast, when cool across the T_c , the specimen will elongate to its original shape as anisotropy increases. The conventional LCE is nonprogrammable; hence, it cannot be included in the SMPs category. Instead, the localized shape change could be achieved by selective actuation.^[63] Ware et al.^[64] imprinted the topological defects in the LCEs film to fabricate the actuator with complex programmable shape changes.

Each individual defect could actuate a localized area of the film either up or down with a cone structure. In another study, the oriented liquid crystal cells were patterned by photoalignment azobenzene dye to localize the response in LCEs.^[65]

To develop LCEs with programmable shape memory behavior, the two-stage thiol-acrylate Michael addition and photopolymerization reaction has been broadly applied in LCE synthesis with fast reactivity and good stability.^[66] In place of the cooling process during the shape memory programming process, the photo-crosslinking method was used to fix the temporary shape of the liquid crystalline network^[67] (Figure 5a).

The photoinitiator was added to the LCE synthesis route, which reacted with other elements in the polymer under UV light irradiation to fabricate a network that locked the temporary shape. This method allowed the transformation of the LCE into different complex temporary shapes^[10] (Figure 5b). The introduction of an exchangeable disulfide bond in the LCE synthesis helped develop a reprogrammable liquid crystalline network.^[50,67,68] Moreover, Xiao et al.^[69] demonstrated the complex shape morphing of a uniaxially oriented LCE strip. Reversible locomotion was achieved between designed 3D shapes to construct electrically powered soft robots. The

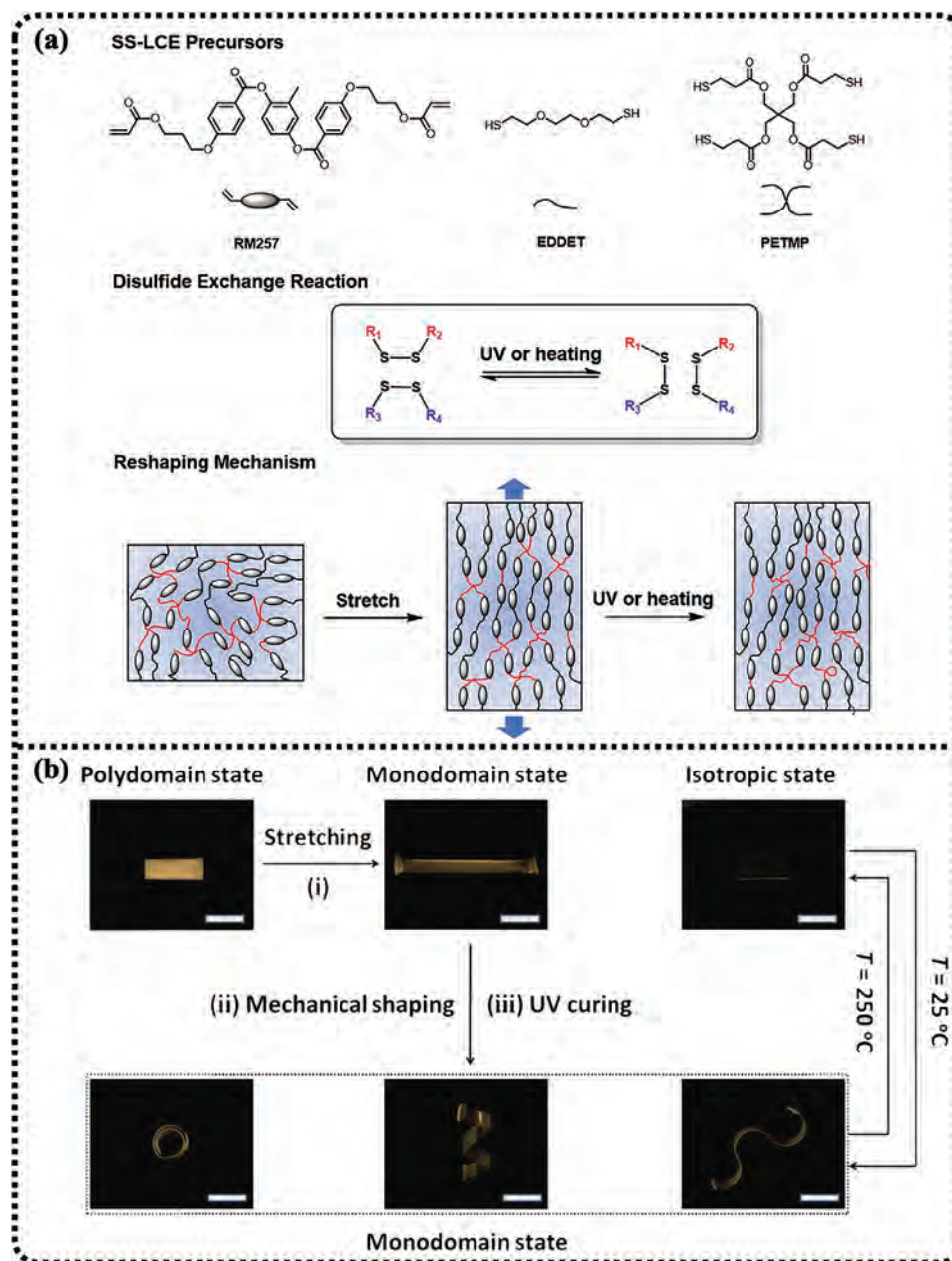


Figure 5. a) Design of the disulfide liquid crystalline elastomer (LCE) and illustration of the dynamic network of the LCE under UV irradiation or heating. Reproduced with permission.^[67] Copyright 2017, American Chemical Society. b) Programming and reversible shape memory effect of LCE synthesis with diacrylate RM82. Reproduced with permission.^[10] Copyright 2018, Wiley-VCH.

programming procedures and the underlying fundamental mechanisms are similar for both the shape memory semicrystalline polymer and LCE, which require internal stress to direct the changing of the molecular anisotropy in the phase transition process. Based on this principle, two-way SMPs with better mechanic property and adjustable shape-transforming temperature can be developed to meet the complex application requirement, especially for the biomimetic materials and soft robotics.

2.5. Multiple SMPs Mechanism and Classification

Multiple SMPs can attain more than one temporary shape in each shape memory cycle. This phenomenon is derived from the step transition behavior in the polymer. The multibranch model based on the SLS thermoviscoelastic theory was used in the quantitative analysis of the multishape memory effect.^[70] This model captured the complex relaxation behavior in the polymer. Fixation of the different temporary shapes in multiple SMPs requires deforming in the corresponding interval transition temperatures, and the process is referred to as the multiple-step programming. For instance, a two-step programming is required for triple SMPs with two temporary shapes. According to the same principle mentioned above, this concept can be extended to different multiple SMPs, such as quadruple SMPs or quintuple SMPs. Based on various mechanisms and molecular structures, multiple SMPs are categorized into three groups: multiple SMPs based on separated phase transition, those based on single broad phase transition, and those based on molecular switches.

2.5.1. Multiple SMPs Based on Separated Phase Transition

The scientific design of the different molecular segments allows a copolymer to exhibit multiple shape memory effects due to the separated transition temperature of different sectors. Lendlein et al.^[71] developed a triple-SMPs system with two temporary shapes in one shape memory cycle in 2006 (**Figure 6a**). It comprised two SMPs system: (1) the PCL containing poly(cyclohexyl methacrylate) (PCHMA) segments, and (2) the PCL containing poly(ethylene glycol) (PEG) segments. $T_{m,PEG}$ increased from 17 °C to 39 °C with the growing PEG segments. $T_{m,PCL}$ was about 50 °C, while $T_{g,PCHMA}$ was 140 °C. Shape recovery occurred at different transition temperatures in both these systems. Magnetic particles were introduced into the polymer system in the later designs to achieve remote actuation in triple SMPs.^[72] A good multi-shape memory effect occurred when the concentration of the PEG segment content ranged between 50% and 70%. These studies constituted a general triple-SMPs synthesis idea of combining two different one-way SMPs with different T_{trans} , which was applied to the development of reversible triple-SMPs in 2010.^[73] The developed copolymer networks contained two segments, PCL and PPD. Different segments created discrete T_{trans} in the polymer ($T_{m,PCL}$ 33–40 °C and $T_{m,PPD}$ 75 °C) playing a critical role in the triple shape memory effects. A reversible shape transition behavior was observed between T_{high} and T_{low} as well. Various

copolymers with multiple shape memory blocks have been successfully synthesized based on different molecular segments.^[74] In this regard, the poly(p-dioxanone) (PPDO)–PEG network exhibited triple shape memory effects at 70 °C and 120 °C.^[75] Additionally, self-healable and recyclable multiple SMPs that contained PPDO and poly(tetramethylene oxide)-glycol segments were developed.^[76] In another study, Wang et al.^[77] combined the glass transition and melting transition to design triple SMPs with cinnamon groups (**Figure 6b**). Furthermore, the cold drawing process could replace the multiple deformation process in the shape memory programming step^[78] based on previous research in which the one-step programming possibility was confirmed.^[79,80] Cold drawing constitutes a one-way deformation procedure at ambient temperature. This process is a creative method that simplifies the programming process in multiple SMPs.

The polydomain-monomodomain transition (156.3 °C and 172.5 °C) and a glass transition (80 °C) were combined to create a liquid crystalline polymer.^[81] This polymer exhibited triple shape memory effects as well as the reversible shape memory effect due to the liquid crystalline segments. Li et al.^[82] incorporated the smectic liquid crystal segments in the polylactic acid (PLA) main chain (**Figure 6c**). Both the transitions of the polymer were linked with the mesogenic domain in the polymer, making it challenging to tune two-phase transition temperatures independently. Thus a shape memory main network with a liquid crystalline side chain was synthesized by the ring-opening metathesis polymerization with the Grubbs catalyst method.^[83,84] The triple shape memory effect of the polymer network was derived from the glass transition of the main network (22.5–32.1 °C) and the anisotropic-isotropic transition (94–103.5 °C) of the side domain corresponding to different methylene spacer length between the polymer backbone and the cholesteryl side chain. The separately chosen side domain and main chain allow independent tuning of the two transition phases.

The interpenetrating polymer network (IPN) also exhibits multiple shape memory effects. IPN consists of a blend of two individual networks in an interpenetration model that involves a more complex synthesis approach than the simple blending method. Two different reactions were employed and coordinated in the construction of its structure. Its triple shape memory effect was based on PPDO and PCL that correspond to the crosslinked network and supramolecular network, respectively.^[85] The temporary shape and the recovery shape were both programmed at 55 °C and 110 °C. Increasing the PPDO network ratio was beneficial to the shape recovery property since the network created by covalent bonds was more reliable compared to the network with hydrogen bonds. Additionally, the crystallization ability of the PCL and PPDO segments was enhanced compared to the co-network.

The multiple shape memory effect can be achieved without a good dispersion of different polymers in the same network. For instance, a nonwoven PCL (T_m 35 °C) membrane was fabricated after it was electrospun into the epoxy matrix (T_g 55 °C).^[86] Its triple shape memory effects originated from the interaction between the melting transition of the PCL and the glass transition of the epoxy. Well-separated transitions were observed

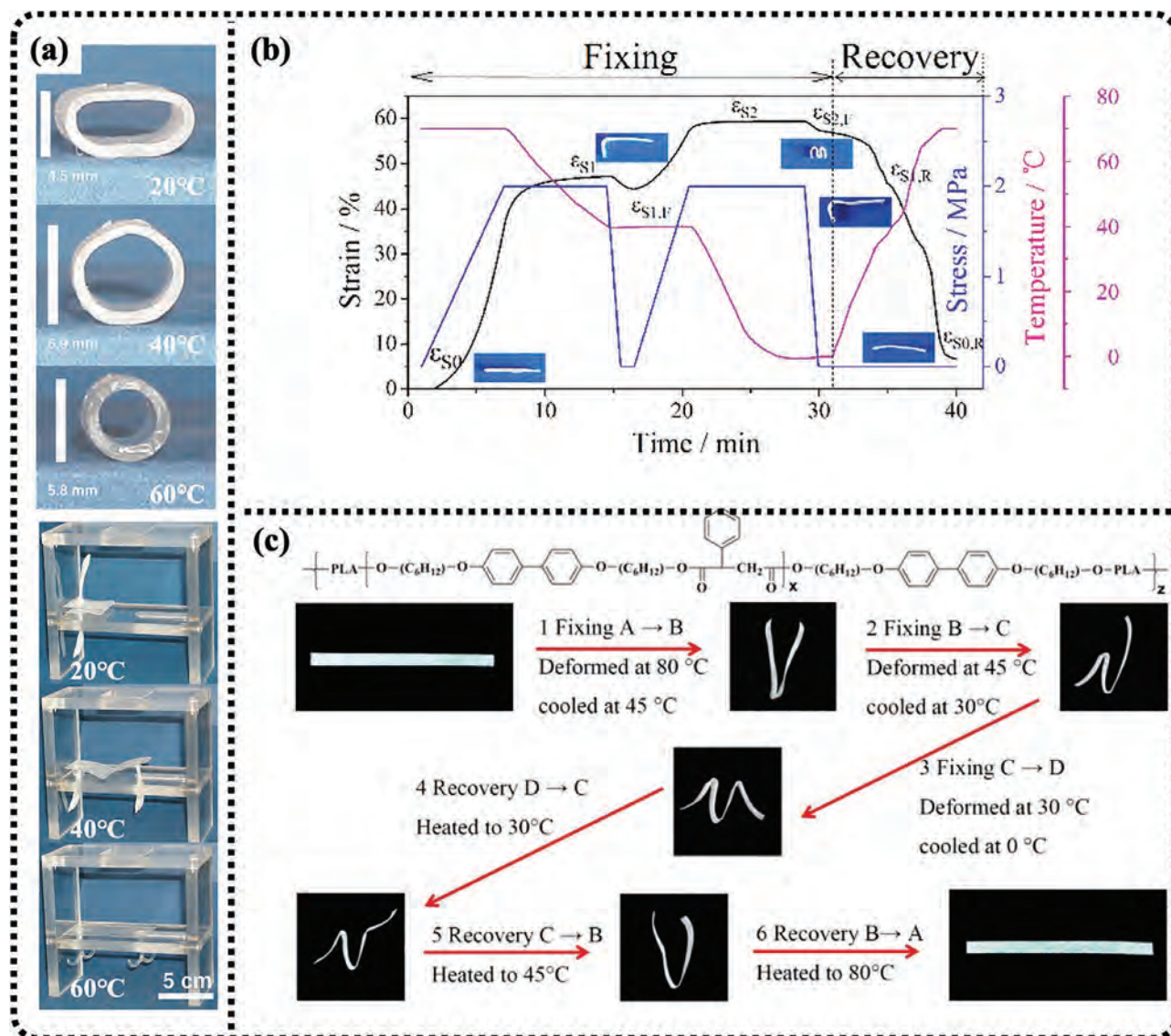


Figure 6. a) Photographs illustrating the triple-shape effect. A tube and a plate with anchors were heated upon 60 °C. Reproduced with permission.^[71] Copyright 2006, National Academy of Sciences, USA. b) Demonstration of triple-shape memory effect polyurethane with dynamic mechanical analysis. Reproduced with permission.^[77] Copyright 2013, American Chemical Society. c) Molecular structure and quadruple shape memory effect poly(lactic acid) (PLA)-based copolymers containing the smectic liquid crystal. Reproduced with permission.^[82] Copyright 2016, American Chemical Society.

during the shape recovery process. The SMPs were later laminated with a well-separated T_g into a bilayer structure. Besides, the dicumyl peroxide (DCP) crosslinking approach was employed to create PE blends with triple and quadruple shape memory effects.^[15,87] Moreover, doping the small molecules into the SMPs network is an ideal way of creating multiple SMPs based on the noncovalent bonding between the small molecules and the main polymer network.^[88–90]

2.5.2. Multiple SMPs Based on Single Broad Phase Transition

Polymers with a single wide T_g range can meet the requirements of the multiple shape memory effect. The transition region will be fixed as the polymer is synthesized for the multiple SMPs with

separated phase transition temperature. The adjustment of the transition temperature requires the synthesis of a new polymer. Instead, the deformation temperature can be selected based on the requirement of the applications in the multiple SMPs with a single broad transition temperature. Nafion, a commercial thermoplastic polymer with poly(tetrafluoroethylene) and perfluoroether sulfonic acid segments, possessed a single broad transition temperature ranging from 55 °C to 130 °C^[91] (Figure 7a). This allowed multiple programming at different temperatures inside the extensive phase transition region. Nafion was deformed into a temporary shape A at 140 °C, fixed at 68 °C, and distorted into temporary shape B. After it was fixed at 20 °C, its membrane was reheated to 140 °C, and the deformed shape changed to the initial permanent shape from two temporary shapes. The deformation temperature was selected based on the actual need.

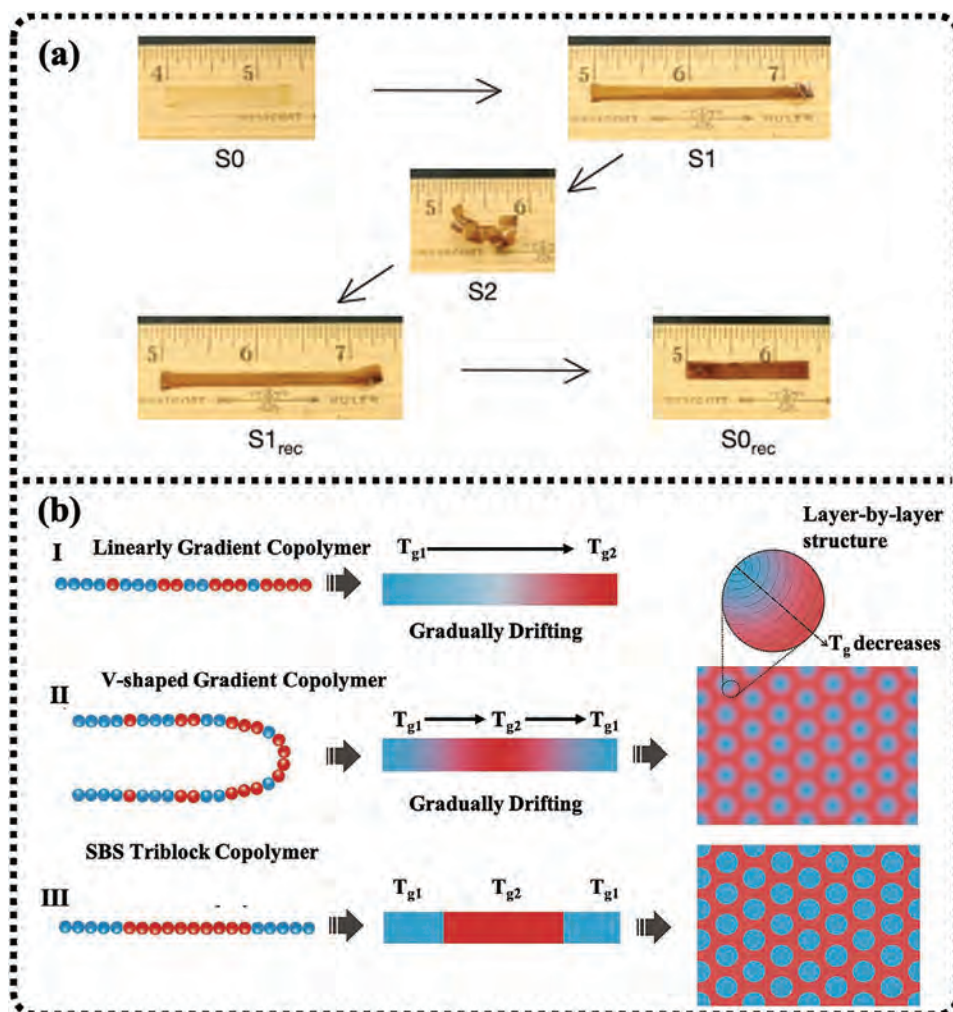


Figure 7. a) Triple shape memory behavior of perfluorosulfonic acid ionomer. Reproduced with permission.^[91] Copyright 2010, Springer Nature. b) The molecular design strategy for multiple SMP. I: Chain architecture of a linear-gradient copolymer. II: Chain architecture and microphase separation of a V-shaped gradient copolymer. III: Chain architecture and microphase separation of the styrene–butadiene–styrene (SBS) triblock copolymer. Reproduced with permission.^[92] Copyright 2012, Wiley-VCH.

Thus, triple and quadruple shape memory effects could be realized within a single shape recovery cycle.

To fabricate a polymer that possesses single broad phase transition, the symmetric gradient copolymer of styrene (St) (T_g 100 °C) and methyl acrylate (MA) (T_g 18 °C) was used to determine whether polymers exhibited multiple shape memory effects.^[92] The polymer was synthesized by the controlled living radical emulsion copolymerization technique, which involved the growing process of the polymer chain being gradually added by the monomer (Figure 7b). This process avoided the separation of $T_{g,high}$ and $T_{g,low}$ segments. The product with a broad T_g range between 20 °C and 103 °C adopted a V-shape configuration, implying that in both ends the St segments constituted a high T_g , while in the central part, the MA represented a low T_g . The gradual transition from $T_{g,high}$ to $T_{g,low}$ occurred due to changes in the St and MA fed ratio in the polymerization process. Thus, the polymer was capable of producing quadruple and quintuple shape memory effects. Controlled/living radical emulsion copolymerization could become the most

fundamental approach for synthesizing multiple SMPs because of the diversity of monomers and the precise synthesis process of the polymer chain.

The semi-IPN network with the poly(methyl methacrylate) (PMMA) and PEG segment exhibited multiple shape memory effects in the study conducted by Li et al.^[93] Incorporation of PEG into the PMMA network broadened the T_g of the whole polymer. The change of the PEG/PMMA ratio altered the transition temperature, causing the quintuple shape memory effect as the T_g region turned from 45 °C to 125 °C. Grafting of the PU chains onto the poly(vinyl alcohol) (PVA) allowed the polymer to possess a broad T_g range from 25 °C to 75 °C.^[94] Furthermore, this polymer showed a water-induced shape memory effect in the shape recovery process. The PVA segment constituted a hydrophilic material. Therefore, as the polymer was soaked in water, it swelled, causing movement of the molecular chain and resulting in a broader T_g range.

For the thermomechanical theory of multiple SMPs, the broad transition region can be regarded as the collection of a

continuous sharp peak.^[95] Each sharp peak can be viewed as an elemental memory unit (EMU) corresponding to the transition temperature. Only the EMU with T_g below the deforming temperature can be actuated for the programming and recovery process. Thus, the triple, quintuple, quadruple, and other multiple shape memory effects are presented as the polymer possesses a wide range of transition temperatures. T_m contributes to the multiple shape memory effects as well.^[96,97]

2.5.3. Multiple SMPs Based on Molecular Switches

The multiple shape memory effect under nonthermal conditions can be based on different molecular switching methods. A typical example is the incorporation of photosensitive units into the one-way SMPs. The synergistic effect of the glass transition and the photoreversible reaction can produce multiple shape memory effects. Wang et al.^[43] reported a hyperbranched polyester containing ester groups and cinnamic double bonds. The hard cinnamoyl and the soft aliphatic moieties constituted the polymer backbone, which was responsible for the T_g (36 °C to 64 °C). Besides, the cinnamic double bonds comprised the polymer's photosensitive units. In the shape memory cycle, under the UV light irradiation ($\lambda = 280\text{--}450$ nm), the polymer was first deformed into a temporary shape A. Then, it was heated to 70 °C and deformed into a temporary shape B and fixed at 20 °C. The multiple shape recovery process was demonstrated as the polymer was deformed to the temporary shape B after being heated and irradiated with UV light.

The water-sensitive molecular switch has also been applied to the design of multiple SMPs. A combination of the thermal-sensitive and water-sensitive units exhibited triple shape memory effects.^[98] The incorporation of cellulose nanowhiskers into the PCL network through the mixing of the suspension was followed by solidification. The polymer chains were composed of the cellulose nanowhiskers connected via strong hydrogen bonds, which were affected under an aqueous environment. Therefore, it functioned as a water-sensitive unit in the integrated network. The shape memory programming and recovery process involved the cooperation of humidity and temperature changes that corresponded to the different temporary shapes. The full recovery of the temporary shape was achieved in hot water at 65 °C.

An aqueous environment needs to be applied for the shape memory hydrogel since the hydrogel must keep moisture compared to the water-sensitive molecules. A dipole–dipole reinforced hydrogel consisting of poly(acrylonitrile 2-methacryloyloxyethyl phosphorylcholine) units was fabricated through copolymerization.^[99] Zinc ions in the ZnCl_2 solution incorporated with the nitrile lone pair electrons cause the dissociation of the dipole–dipole pairs. The association and dissociation process caused reversible shape deformation. Based on this adsorption mechanism, the temporary shapes were successfully locked according to the different ZnCl_2 solution concentrations. Temporary shapes A and B were fixed in 30% ZnCl_2 and pure water, respectively. The temporary shape recovered when the hydrogel was immersed in 50% ZnCl_2 . This strategy has been extended to a variety of hydrogel containing the dipole–dipole of cyano groups. Moreover, the complex structure programming with

asymmetric structure and potential biomedical applications have been investigated.

3. Actuation Methods for SMPs and SMPCs

Contact heating is the most conventional actuation method for SMPs; however, the response rate is quite low for SMPs with low thermal conductivity. Besides, conventional SMPs have low storage modulus, low shape recovery speed; therefore, they should be modified into composites for productive use in various applications. Herein, we mainly discuss the novel actuation methods for SMPCs, with the multifunctionality originating from the functional fillers. These modification processes, which involve changes in the elasticity, permeability, color, transparency, conductivity, light sensitivity, and shape recovery properties, ensure the polymers gain innovative capabilities compared with the conventional SMPs. Both the thermal and athermal shape memory actuation methods are introduced. Besides, different SMPCs applications that involve aerospace engineering, biomedical devices, flexible electronics, soft robotics, shape memory arrays, and 4D printing have been demonstrated to gain multifunctionality.

3.1. Electroactive SMPCs

The nonconductivity of dry polymers is commonly reflected in SMPs. The fabrication of conductive SMPs can be achieved through the embedding of a variety of conductive factors such as graphene, graphite, $\text{CNT}^{[100,101]}$ (Figure 8a), conductive metal particles,^[102] and conductive polymers^[103] in the SMPs matrix. Since the external contact heat is unfavorable for most applications, these fillers change the conductivity of the material, thereby realizing the remote actuation of shape memory effect with Joule heat generated by energization.

The three critical steps involved in the preparation of a conductive polymer composite are building a conductive 3D network, uniformly doping the conductor unit, and improving the interface bonding between the conductor and polymer matrix. Among the conductive fillers, carbon fillers are the most commonly used in the development of conductive polymer composites. In 2004, Koerner et al.^[54] achieved electro-stimuli shape recovery by incorporating CNT into a PU network. The CNT network enhanced the mechanical property and shape recovery stress of the polymer composite. In a separate study, Cho et al.^[104] introduced conductive carbon fillers, including carbon black and CNT into the SMPs. The polymer filled with 30% carbon black showed conductivity about $1\text{--}10^{-1}$ S cm^{-1} , with the carbon black serving as small conductive particles spread in the polymer. However, besides taking a 30% weight ratio in the polymer composite, these particles could not enhance the strength or toughness of the polymer matrix, making it an unsuitable approach. Conversely, the polymer filled with 5% CNT showed conductivity of about 10^{-3} S cm^{-1} . This is an indication that incorporating the CNT is a better method since a lesser content is required, and it can reinforce the materials. However, to yield better results, CNTs should be uniformly interspaced in the polymer matrix, especially during the

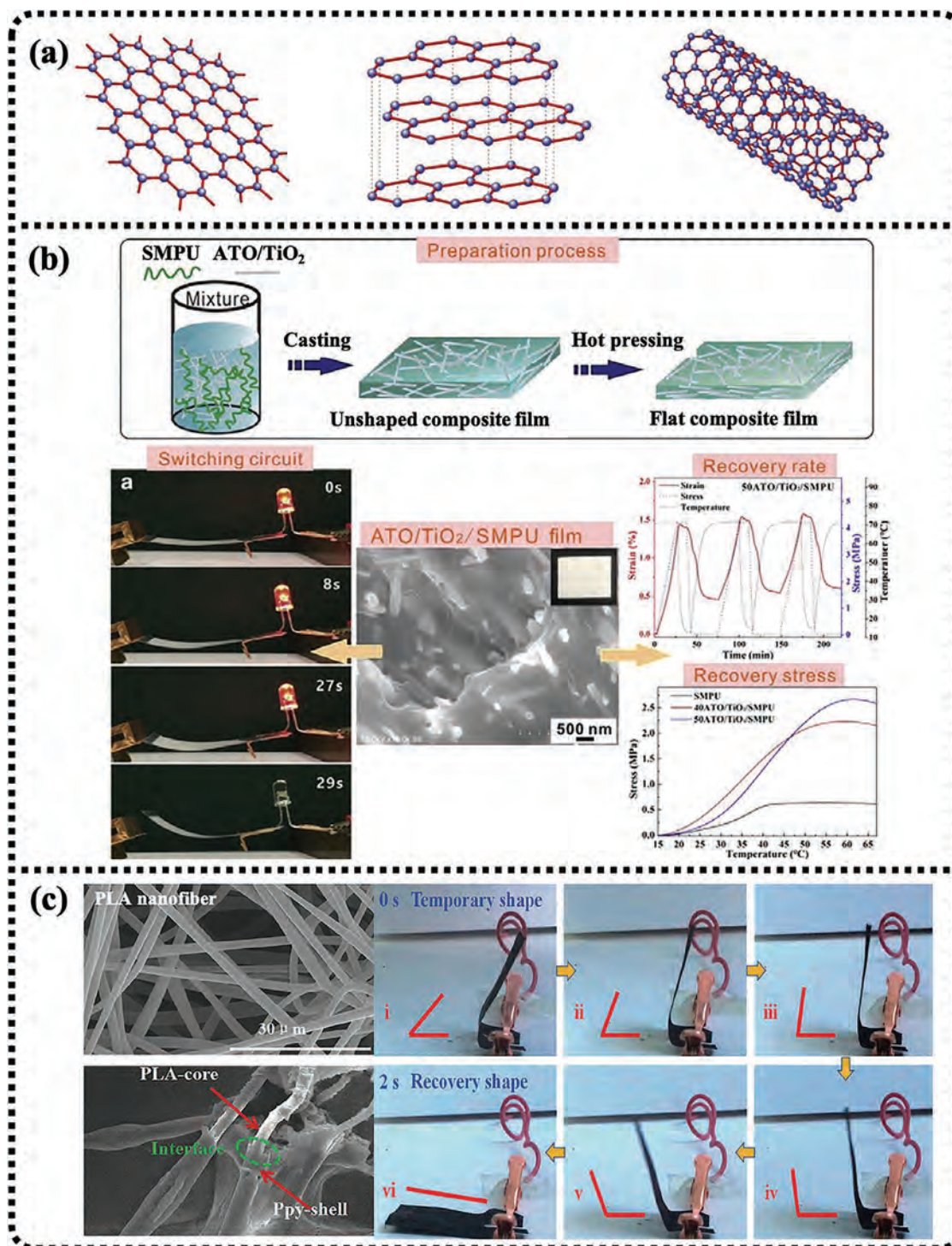


Figure 8. a) Molecular structure of graphene, graphite, and a carbon nanotube (CNT). Reproduced with permission.^[100] Copyright 2018, Wiley-VCH. b) Fabrication process and shape switching behavior of shape memory polyurethane (SMPU) composites. Reproduced with permission.^[16] Copyright 2018, Elsevier. c) Core-shell structure and electro-stimuli shape recovery behavior of PLA-poly pyrrole fibers. Reproduced with permission.^[103] Copyright 2018, American Chemical Society.

curing process, to avoid aggregation of the CNTs.^[105] The surface-modified CNT showed better cohesiveness with polymer matrix, resulting in the enhancement of mechanical properties. However, balancing between the interface cohesiveness

and the conductivity of CNT fillers is needed since conductivity decreases during the surface modification. Wan and co-workers^[106] incorporated CNT with poly(D,L-lactide-co-trimethylene carbonate) to form liquid sensors. Besides, the

effectiveness of carbon nanofiber and graphene in enhancing the conductivity of polymer composites and their mechanical performance has been demonstrated.^[107,108] Coupling vapor grown carbon nanofiber with poly(ethylene-co-vinyl acetate) has also been reported by Qian et al.^[109] Further, the production of electroactive SMPs by the embedding of graphene in PU and PLA has also been reported in detail.^[110,111]

The incorporation of metal particles such as Ni into the polymer has been shown to enhance the conductive network by aligning into conductive chains under the magnetic field.^[102] The connection of Ni chains and carbon black particles significantly reduces the resistivity, hence achieving the electrically triggered shape recovery. Liu and co-workers^[16] applied high-intensity ultrasound to uniform particle dispersion of antimony-doped tin oxide/TiO₂ whiskers coupled with the PU network revealing that shape recovery could be actuated with 70 V DC voltage in 30 s (Figure 8b). In another study, Wang and co-workers^[112] designed a silver nanowire/melamine foams/epoxy SMPs with a 3D conductive network structure. The shape memory behavior of the SMPs could be driven with a low voltage at 3 V in 25 s, which demonstrated excellent electroactive behavior with low resistance compared with most of the conductive SMPs. Besides, the pressing of Ag nanowire substrate with epoxy polymer and PCL layer as well as self-healing and electroactive properties have been published by Luo et al.^[113] Compared with carbon fillers, metal particles generally have better conductivity. Further, the metal has completely different interfacial properties from polymers, making the incompatibility of metals and polymers a significant challenge.

The development of conductive polymeric composite networks has been documented in the literature as well. For instance, Cho et al.^[114] introduced the conductive polypyrrole (PPy) into the SMPs research by immersing a thin PU membrane into the pyrrole solution. The PPy shell was formed on the PU membrane with iron ions as catalysts. The resulting PU/PPy composites showed conductivity of 10⁻² S cm⁻¹, and the electroactive shape memory behavior was actuated upon application of 25 V. Zhang and co-workers^[103] further extended this idea into the nanoscale, where PLA was electrospun into nanofiber membranes and PPy was synthesized on the surface of nanofiber under subzero environment by chemical vapor deposition. Membranes consisting of core-shell fibers were obtained in the experiment with the overlapping nanofiber, providing sufficient conductive paths (Figure 8c). Further, they demonstrated the absence of any side effects in a subzero environment. This method improved the membrane conductivity up to 0.5 S cm⁻¹.

3.2. Magnetism-Driven SMPs

Unlike the direct shape memory driving method, the magnetic field is an indirect way of triggering the shape memory behavior. Most of the magnetism-driven SMPs are based on the embedding of the magnetic particles into the SMPs, typically ferrite and soft magnetic materials, which can generate Joule heat under the magnetic field to cause shape recovery. A Nafion/Fe₃O₄ composite membrane whose shape memory effect was combined with a controllable magnetic trigger was

reported by Zhang et al.^[115] They recorded surface temperatures of about 38–40 °C, which were close to the average body temperature. Since the Fe₃O₄ particles formed visible boundaries with the polymer matrix, the surface modification was required to improve the ferrite oxide distribution and incorporation into the polymer. Lendlein et al.^[17] further integrated the oligo(ω -pentadecalactone) with the magnetic particles. The integrated nanoparticles were crosslinked with polymer precursors during the curing process. Gong and co-workers^[116] also incorporated the ferrite oxide particles into CNT through β -cyclodextrin functionalization, where the incorporated particle was first dissolved in PCL solution before being electrospun into a nonwoven nanofiber. These methods improved the magnetic particle compatibility in the polymer matrix. Furthermore, Ze et al.^[117] reported SMPs that required the shape programming process without stress. In such a case, the Fe₃O₄ and NdFeB microparticles were embedded in an acrylate-based SMPs, and they corresponded to their respective magnetic fields and induced heating and shape deformation separately (Figure 9a). Besides, the SMPs were capable of fast and reversible shape transformation. Testa and co-workers^[118] further demonstrated the use of magnetic fluid as a magnetic material by encasing the magnetorheological fluid liquid droplets into a poly(dimethylsiloxane) (PDMS) matrix based on emulsion procedure. A thermal, reversible, and rapid shape memory behavior was actuated with microstructural transformation under the magnetic field (Figure 9b). A magnetic field is an ideal approach to triggering the shape memory effect since it can penetrate deeply into the bulk polymer. However, compared with the electricity-triggered SMPs, the magnetism-driven SMPs require a strong magnetic field to generate enough Joule heat, which is unfavorable for the human body.

3.3. Light-Driven SMPs

Development of SMPs whose shape memory effect is driven by visible light and infrared (IR) radiation can be achieved by the embedding of gold nanomaterials in the polymers. After crosslinking small amounts of Au particles with poly(ethylene oxide) (PEO) network, Zhang and co-workers^[119] reported SMPs with light-triggered shape memory effect and self-healing property. The shape memory effect characterized by laser exposure ($\lambda = 532$ nm, 7 W cm⁻²) was actuated by the increase in temperature occasioned by the photothermal conversion of the Au particles. Guo and co-workers^[120] incorporated the gold nanoparticles into the poly(D,L-lactic acid) as well (Figure 10a). Besides, similar phenomena have been found in SMPs with gold nanorod embedded.^[121,122] In a separate study, Fang and co-workers^[123] used organic rare-earth complex for light absorption. Yb(TTA)₃Phen and Nd(TTA)₃Phen demonstrated selective photothermal conversion effect under near-infrared (NIR) light of 980 and 808 nm, respectively. Additionally, the incorporation of the organic rare-earth complex into poly[ethylene-ran-vinyl acetate] (PEVA) provided selective NIR light-responsive SMPs. Earlier research has also indicated that CNT is capable of inducing shape memory response under infrared source.^[54] With the silver nanoparticles grafted on cellulose nanocrystal, an SMP with rapid IR response was fabricated by Toncheva

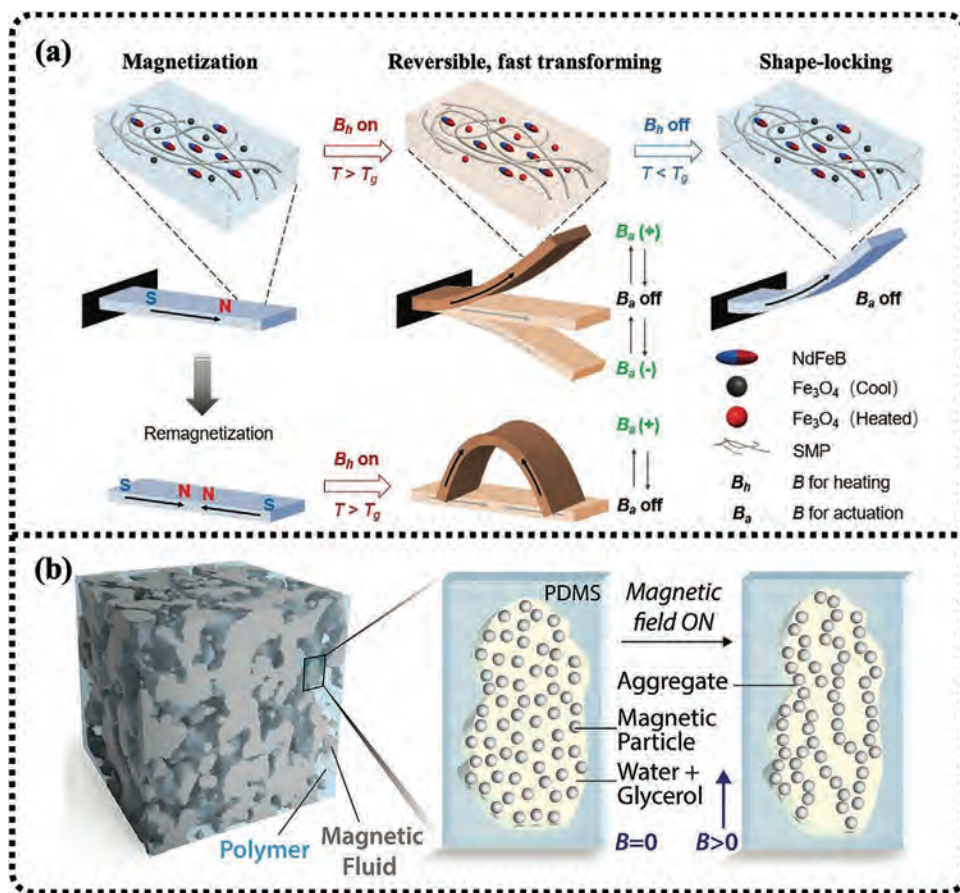


Figure 9. a) Working mechanism of magnetic shape memory polymers (SMPs). The polymer is stiff at room temperature, and it can be softened with a tunable shape under the magnetic field. Reproduced with permission.^[117] Copyright 2019, Wiley-VCH. b) 3D reconstruction of the internal two different phases inside the material obtained from tomography data. Reproduced with permission.^[118] Copyright 2019, Wiley-VCH.

et al.^[124] (Figure 10b). Selective shape memory-driven SMPCs can be achieved by the design of polymers with fillers at different absorption wavelengths, which are vital in complex optical environments. Wu et al.^[125] reported a carbon dot/PVA composite fluorescence shape memory hydrogel capable of triggering the shape recovery process under UV light irradiation from the fluorescence quantum yield of carbon dots. Wang and co-workers^[126] characterized the shape memory behavior at the nanoscale by tuning the polarization direction of linearly polarized light (Figure 10c). Since shape memory transition driven by visible light and IR radiation is based on the photothermal conversion effect and requires deep light penetration and proper particle distribution, its application in a bulk polymer is difficult. The particle concentration ought to be carefully controlled since both the difficulty in dispersion and the high concentration of nanofillers impede light penetration.

As the electromagnetic wavelength increases, the light turns from visible into the microwave, which follows the same absorbing principle as light. The carbon-based material then transforms the microwave into heat vibration. Yu et al.^[127] incorporated the CNT with shape memory resin, successfully inducing the shape memory effect with microwave radiation (40 W, 2.45 GHz). The relationship between microwave absorption ratio, microwave frequency, and CNT concentration has

also been studied. Kalita and co-workers^[128] loaded the Fe_3O_4 nanoparticles on CNT by surface modification, and synthesized the crosslinked CNT/ Fe_3O_4 with hyperbranched polyurethane. The resulting thermoset composite showed an excellent shape memory property under the microwave.

3.4. Solution-Driven SMPCs

In 2005, Huang et al.^[129] reported a unique shape memory phenomenon of polyurethane wire. Unlike the conventional heating recovery, the polyurethane could revert to its original shape after immersion in water for 30 min under room temperature through a phenomenon known as the plasticization effect. During the immersion, water molecules were absorbed into the polymer chain, which in turn softened its molecular interaction through hydrogen bond and then triggered the swelling process, thus decreasing the polymer T_g . Subsequently, the PU wire fully recovered without any external heating. For the SMPs research, the shape memory effect with the nonthermal heating process and without chemical reactions is a novel area that deserves further exploration.^[130] Du and Zhang^[131] studied the swelling effect on shape memory crosslinked PVA through the deformation of the PVA sample under 80 °C in the dry state. The sample

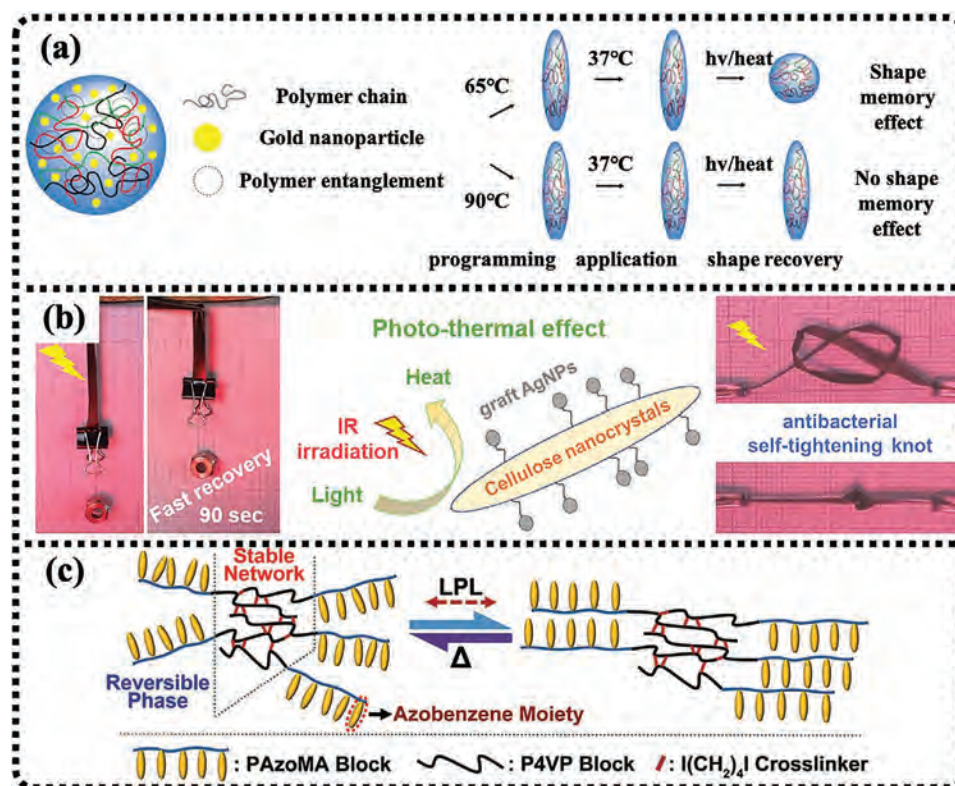


Figure 10. a) Poly(D,L-lactic acid) particles were fabricated encapsulating hydrophobic lipid stabilized gold nanoparticles followed by stretching under low and high temperatures. Reproduced with permission.^[120] Copyright 2018, American Chemical Society. b) Poly(ϵ -caprolactone) (PCL)-based shape memory polymer (SMP) actuated upon infrared (IR) illumination. Reproduced with permission.^[124] Copyright 2018, American Chemical Society. c) Schematic illustration of change of polymer chain conformations in a two-phase system of shape memory porous film. Reproduced with permission.^[126] Copyright 2018, Wiley-VCH.

returned to the original shape after immersion in water for 45 min under room temperature. The differential scanning calorimetry (DSC) measurement demonstrated that the T_g of PVA decreased sharply in water. Liang et al.^[132] developed a smart hydrogel with high stretchability, self-healing property, and shape memory behavior. The hydrogel was made from the interpenetration of the network structure comprising polyacrylamide and phenylboronic acid grafted alginate, and its shape memory behavior was characterized by dehydration and rehydration.

Although plasticization has been shown to work for hydrophilic polymer,^[133] the water molecules have failed to intrude into the network of hydrophobic polymers. Therefore, the addition of hydrophilic fillers is an ideal way to enhance SMPCs plasticization further. Zhou and co-workers^[19] incorporated microcrystalline cellulose into the PLA matrix that was biocompatible. This resulted in the shape recovery temperature of PLA from 70 °C to 37 °C in water, which was suitable for biological applications. Wang et al.^[134] introduced sodium dodecyl sulfate (SDS), an amphiphilic molecule with the ability to adsorb water molecules into an epoxy SMP. Diffusion then caused epoxy/SDS composite's initial shape recovery after 30 min in water. The shape recovery behavior and storage modules can be optimized by adjustment of the SDS concentration.

pH-induced shape memory response based on the protonation and deprotonation process was also reported in SMPCs by Han and co-workers in 2012.^[135] They combined modified alginate with β -cyclodextrin and diethylenetriamine that worked as

switchable segments. The resulting polymer composite became soft and easy to deform in an aqueous solution with pH 7. When the polymer was bent and quickly placed into a solution with pH 11.5, it maintained the temporary shape perfectly. However, when placed back in pH 7, the polymer returned to its initial shape after 2 min. Since it is biocompatible, biodegradable, and pH 7 is close to human body fluid, this polymer composite has shown great potential in biomedical devices. Zhou and co-workers^[136,137] demonstrated other pH-induced SMPCs. Khoury and co-workers^[138] reported a shape memory effect of a protein-based hydrogel, which consisted of bovine serum albumin. The protein hydrogel could stay in an immobilized programmed shape in tris(bipyridine) ruthenium (II) chloride solution. However, transferring the protein hydrogel to a guanidinium hydrochloride solution led to the loss of stiffness and shape recovery. A multiresponsive hydrogel could be triggered with moisture, and the pH value was demonstrated by Zhang et al.^[132] Two interpenetrating polymer chains consisted of polyacrylamide, and phenylboronic acid grafted alginate gave hydrogel high stretchability and excellent self-healing property^[132] (Figure 11).

4. Recent Advances in Applications of SMPs and SMPCs

Controllable active deformation makes SMPs and SMPCs capable of carrying different components from nanoscale to macroscale.

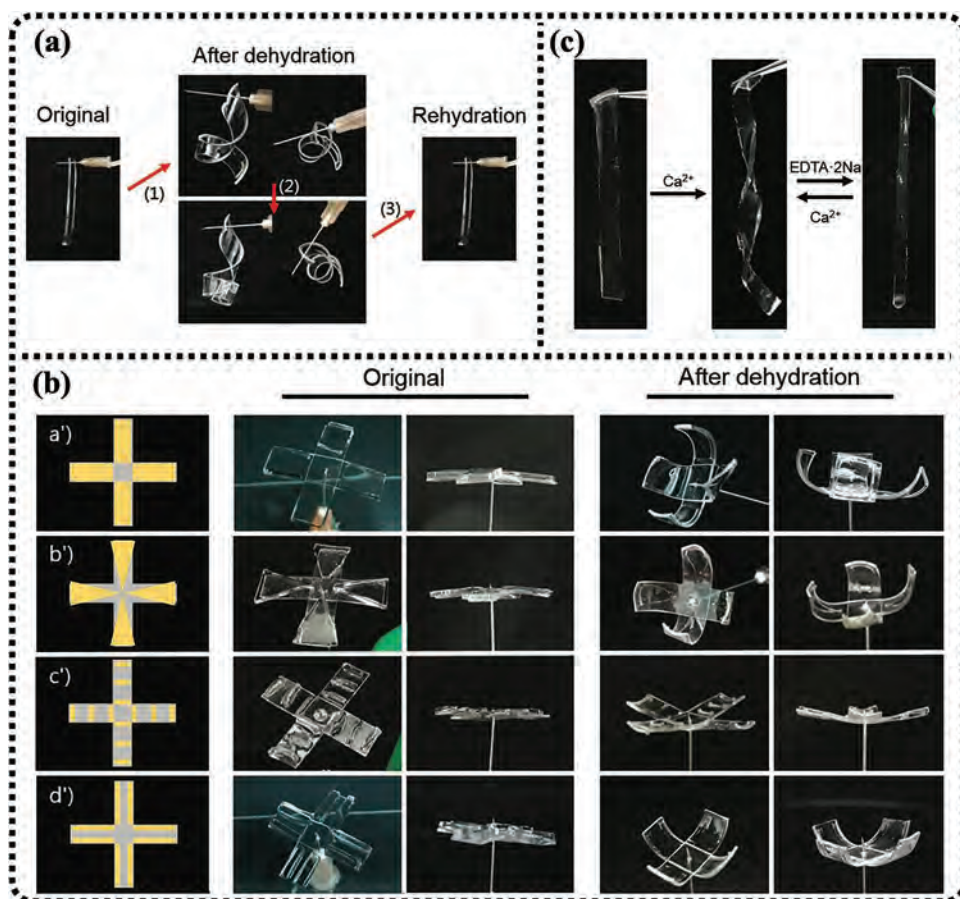


Figure 11. a) Deformation process of Janus assembly containing hydrogel and hydrophilic PDMS during dehydration and rehydration. b) Diverse patterns of plastic flowers. c) The reversible shape memory effect occurring in the presence of Ca^{2+} can be erased by immersion in EDTA-2Na solution. Reproduced under the terms of the CC-BY Creative Commons Attribution 4.0 International license (<https://creativecommons.org/licenses/by/4.0>).^[132] Copyright 2015, The Authors, published by Wiley-VCH.

SMPs/SMPCs-based deployable spacial structures, drug release systems, and 4D printing have been intensively developed. The combination of shape memory behavior and microphase structure transition can achieve the tunable transparency and color control for SMPCs. Besides, self-healing is achieved as the polymer transforms from a hard state to a soft state.

4.1. Aerospace Engineering

SMPCs are lightweight, low-cost, and able to produce active deformation, which are essential characteristics for use in aerospace engineering, especially in deployable structures.^[13,139] Typical examples include SMPCs hinges, gravity gradient booms, deployable panels,^[140,141] (Figure 12a) and reflector antennas. Unlike the traditional metallic hinges^[142] that take up a lot of space and weight, SMPCs hinge reinforced with carbon fiber plain-weave fabrics have been developed^[143,144] (Figure 12b). Shape recovery experiment for analyzing the feasibility of the hinge showed that the hinge displayed a shape recovery ratio of about 100%, and could actuate a prototype solar array during the shape recovery process. In satellites, gravity gradient booms are the main components that support the tip payloads. Conventionally, such

booms as extendible booms and collapsible truss booms are mainly actuated by motors. Zhang and co-workers^[145,146] developed an SMPC truss boom consisting of 18 pieces of laminate tapes that could effectively replace the conventional booms. The epoxy-based SMPCs truss boom was programmed to an “M” shape before the experiment; the boom could be gradually deployed at 80 s during the shape recovery testing. Additionally, the SMPCs-based hinges and booms can be connected with other aircraft components to create different deployable structures such as solar arrays and antennas, which should be packed prior to launching and release in the space. For example, Herath et al.^[147] fabricated a step deployable solar panel array for satellites (Figure 12c). The solar panel was capable of producing step shape recovery under light irradiation. Liu et al.^[148] designed an integrative self-deployable hinge for a gripping device and multi-angle imaging system, which adopted symmetric arc-shaped laminates to save the complex mechanical connections. Simulation result at 100 °C was demonstrated, indicating different levels of maximum von Mises stress distribution as the bending angle altered (Figure 12d). Furthermore, a smart “bamboo” releasing system that applied a bilayer cylinder structure to release payload under mechanic vibration stably was developed by Wei et al.^[149] To further develop the extensive scale payload deploy system, a

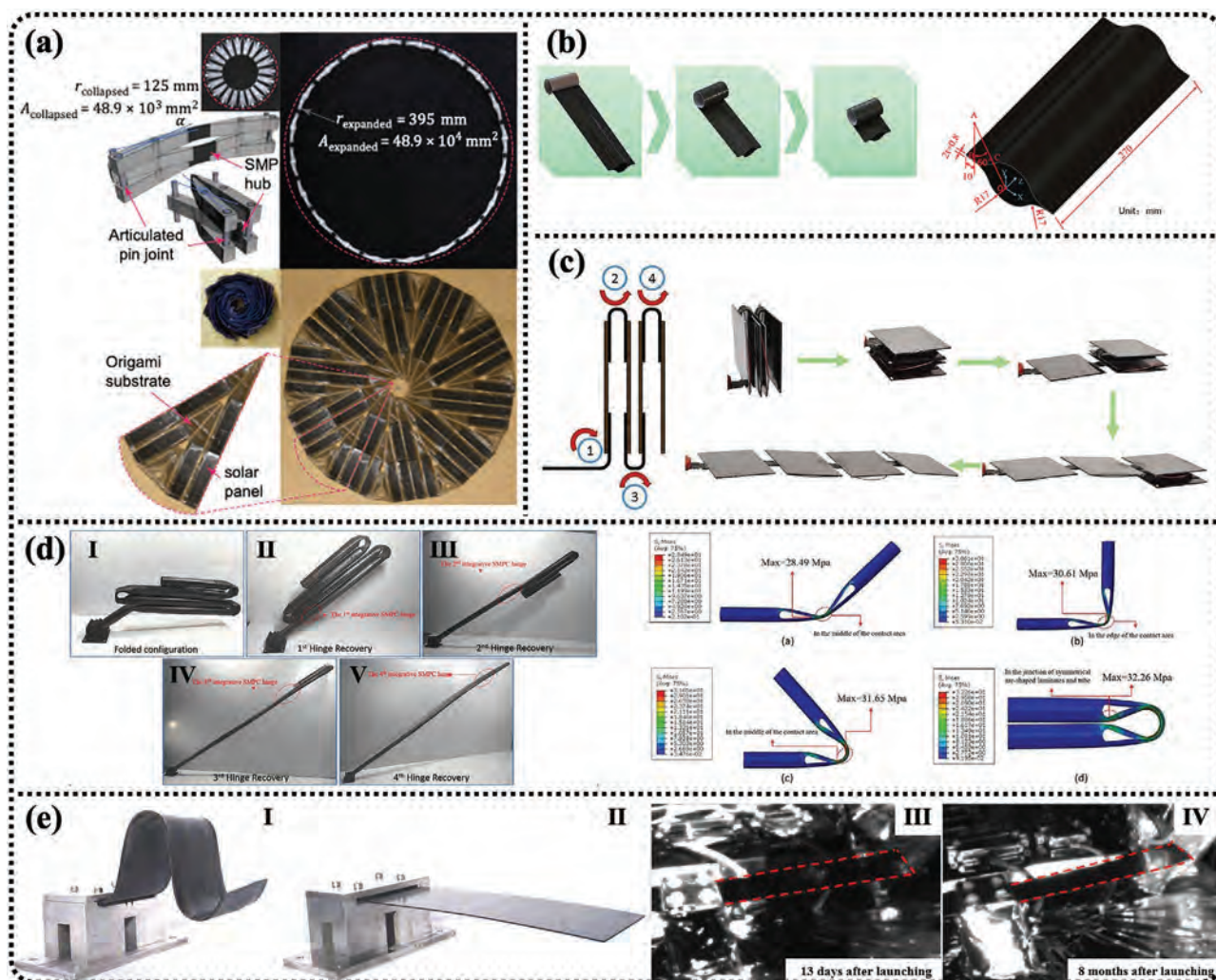


Figure 12. a) A fabricated specimen of the scissor mechanisms and of the origami substrate in both collapsed and expanded configurations, showing ten times change in area. Reproduced under the terms of the CC-BY Creative Commons Attribution 4.0 International license (<https://creativecommons.org/licenses/by/4.0/>).^[140] Copyright 2019, The Authors, published by American Physical Society. b) Model and dimension of the lenticular collapsible composite tube. Reproduced with permission.^[144] Copyright 2019, Elsevier. c) Deployable solar panel array for a satellite with step recovery under near infrared (NIR) irradiation. Reproduced with permission.^[147] Copyright 2018, Elsevier. d) Multiple-shape recovery behavior of the self-deployable structure and von Mises stress distribution bent with different angles I: folded configuration, II: first hinge recovery, III: second hinge recovery, IV: third hinge recovery, V: fourth hinge recovery. Reproduced with permission.^[148] Copyright 2018, Elsevier. e) The configuration of Mission SMS-I, I: packed configuration, II: deployed configuration, III: oblique view of the first observation, IV: oblique view of the third observation. Reproduced with permission.^[153] Copyright 2019, IOP Publishing Ltd.

complex cubic deployable support structure was constructed by Li et al.^[150] Its repeatable cubic unit consisted of SMPCs, and connectors could be assembled into the support structure to meet diverse requirements. Zhang et al.^[151] demonstrated an ultra-lightweight releasing system integrated with resistant heaters. An ultra-lightweight releasing system capable of working under 3 V DC was introduced to the solar array deployed on a CubeSat. The multiple shape programming test and vibration test were carried out to evaluate the feasibility of the releasing system. During the BION-M1 mission in April 2013, the shape memory experiment was carried out with an epoxy foam in the space environment^[152] indicating that applying a porous SMP structure was accessible for aerospace technologies. The SMPCs could be used as structures to support such functional components making them deployable in a space environment. In 2016,

sunlight-stimulated shape memory substrate, known as Mission SMS-I, was launched to the geostationary orbit with an experimental satellite for deployable and long-term anti-cosmos irradiation experiments.^[153] The Mission SMS-I is one of the Chinese pioneering orbital experiments on SMPCs and the world's first SMPCs space flight experiment in a geostationary orbit. The substrate was able to revert from a bent shape to a flat shape under sunlight and it recorded a recovery ratio of almost 100% after 13 days of its launch. Besides, the straight flat configuration was maintained for 8 months without any visible cracks (Figure 12e).

The performances of SMPCs during ground-simulated space environments, including high vacuum, thermocycling, cosmos irradiation, and atomic oxygen, have also been studied to verify their reliability.^[154] In a long-term study of UV radiation and thermo-cycling effect, Tan et al.^[155] applied 80–240 h UV radiation

and $-100\text{ }^{\circ}\text{C}$ to $100\text{ }^{\circ}\text{C}$ thermocycling to the shape memory epoxy. The maximum total mass loss was below 1% while the mechanical property improved, indicating the epoxy's excellent resistivity to the UV radiation and thermocycling. Jang et al. further studied the property change of carbon fiber-reinforced epoxy with UV light irradiation under a vacuum state.^[156] The experiment demonstrated that the storage modulus increased initially as the UV light induced the crosslinking of polymers and it decreased during more protracted irradiation. Notably, a higher shape recovery stress was observed with little change in the shape recovery ratio under 21 h of vacuum UV irradiation. Leng et al.^[157] also reported the effect of atomic oxygen on epoxy-based SMPs. The results indicated that the atomic oxygen had little influence on the storage module and transition temperature, but the mechanical property decreased due to microcracks caused by atomic oxygen erosion.

Aircraft morphing is the smooth transformation from one structure configuration to another configuration. Current morphing aircraft materials involve shape memory alloys, piezoelectric materials, electroactive materials, and SMPCs. SMPCs are considered suitable materials to achieve the morphing of aircraft due to the distinct changes in stiffness and lightweight.^[158,159] Keihl et al.^[160] investigated the possibility of using SMPCs as morphing aircraft structures. Based on testing results of the shape memory and mechanical properties, SMPCs showed the excellent potential to work as a skin material. A variable camber morphing wing structure was developed by Sun et al.^[161] The shape memory morphing skin served as both a shape-changing unit and the aerodynamic fairing. In further research, 20 vol% elastic fiber was embedded into the pure SMPs matrix giving the shape memory wing improved toughness, enhanced strength, and reasonable shape recovery rate.^[162] The research indicated that the cambered wing with SMPCs is the skin-realized morphing to induce airplanes to take off and land.

4.2. Biomedical Devices

The active deformation ability has increased SMPCs' applications in the biomedical fields, such as surgical and vascular applications for the replacement of hand-held surgery instruments.^[163] In 2002, Lendlein et al.^[164] developed a biodegradable SMPs surgery fiber prototype that would be heat-induced to shrink and tighten the wound after suturing (Figure 13a). In their study, Ortega et al.^[165] developed a shape memory foam for aneurysm treatment. The foam was initially compressed during the shape programming process and then transferred to the aneurysm by a catheter. The foam then expanded and filled the distended intracranial aneurysm during the shape recovery process. In a subsequent aneurysm occlusion in vivo test in a rabbit elastase model, Herting et al.^[166] found that a coil coated with a porous SMP foam could promote neointima formation in the aneurysm neck, which in turn led to a full recovery. Metzger et al.^[167] also demonstrated the treatment of ischemic stroke by pitching through the blood clot with a catheter containing SMPs wire. After the SMPs wire was pushed from the catheter into the clot, it recovered a coiled state; hence to pull the clot out and relieve the ischemia became easier. Maitland et al.^[168] investigated a microgripper with laser jaws

activated by SMPs. The microgripper could be positioned with a catheter, thus releasing the captured device inside the vascular. In another research, Maitland et al.^[169] used an SMPs dialysis needle adaptor to reduce thermodynamic stress. The expanded SMPs adaptor had a tubular shape; hence it could be deployed and retrieved by the dialysis needle. The computational simulations and prototype in vitro model showed that the expanded SMPs adaptor reduced the hemodynamic stress on a graft wall, and this might prevent graft failure. Melocchi et al.^[170] embedded an expandable helix SMPs structure into capsules to develop a potential gastric device that expanded to the original shape in aqueous fluids at $37\text{ }^{\circ}\text{C}$. A 4D-printed biomedical occlusion device designed by Lin and co-workers^[171] was used to treat the atrial septal defect. An in vivo feasibility study under a magnetic field was applied to the transformation of the occlusion device (Figure 13b). In a separate study, Wache et al.^[172] developed the SMPs-based stent that could be inserted into the blood vessel. Compared with the conventional narrow metal stent, the polymer could expand after insertion into the specific area, thereby allowing better blood circulation.^[172] Shin et al.^[173] successfully grafted a shape memory tube into the porcine femoral artery with a diameter of less than 3 mm. The surface modification and diffuser design were based on computer modeling to minimize the tissue damage; in addition, because of the shape memory effect, the physical occlusion caused by thrombosis was prevented (Figure 13c).

SMPs have also been applied in surgical procedures. Buckley et al.^[174] fabricated SMPCs in flower and collapsed shapes with Nickel Zinc ferrite loaded. The device was able to expand when exposed to a fluctuating magnetic field. Particle loading of up to 10% volume content could help achieve the fast shape recovery response. In another study, Yamagishi et al.^[175] investigated an ultrathin shape memory nanosheet that could be injected with a syringe and later unfold in $37\text{ }^{\circ}\text{C}$ water. The nanosheet guided by a neodymium magnet in the water employed a bilayer structure, which involved a magnetic particle embedded in the polymer layer and poly(lactic-co-glycolic acid) layer. Conventional surgery devices such as a suture or stent need direct heating, which is not applicable inside the human body; therefore choosing an appropriate deforming stimulus method is necessary. Remote actuation usually involves the embedding of different fillers that can diffuse into the blood, followed by polymer degradation. Therefore, biocompatible fillers deserve to be explored further.

The controllable drug release system can also be developed with SMPCs. Unlike surgical devices, the SMPCs encapsulate and release the actuator in a drug release system. Typically, the drug is loaded in SMPCs after being immersed in a drug solution. Once the polymer swells in water and drug molecules fill the SMPCs, the drug-loaded SMPCs are then obtained after subsequent drying.^[176] Wischke et al.^[177] evaluated the suitability of the SMPs matrix in the drug release system. Drugs such as enoxacin, nitrofurantoin, and ethacridine lactate were dispersed into different organic solutions with the polymer. The results revealed that the incorporation of drugs into the polymer network did not affect the T_g and mechanical properties of the polymer. Serrano et al.^[178] reported a biodegradable hydroxyl-dominant polydiolcitrate whose shape recovery could be induced from $22\text{ }^{\circ}\text{C}$ to $36.6\text{ }^{\circ}\text{C}$. They loaded dichlorofluorescein on the polymer by swelling it in ethanol and distilled water before

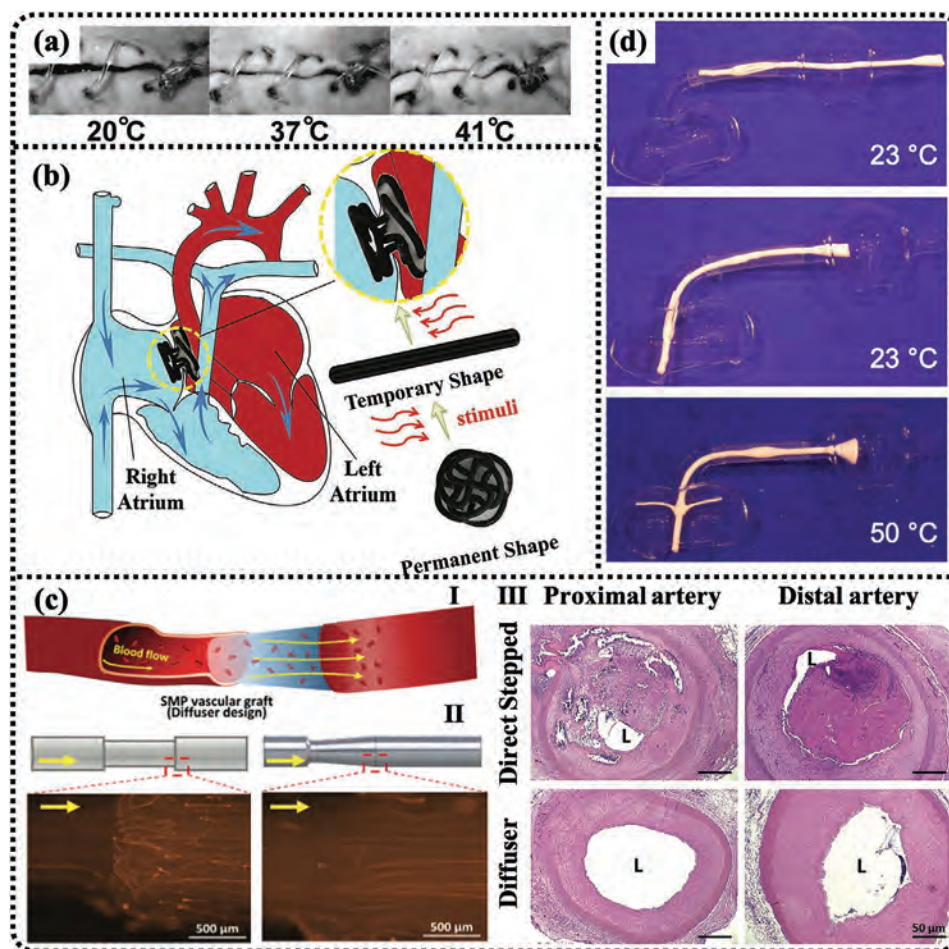


Figure 13. a) Degradable shape memory suture for wound healing. An animal experiment showed the shrinkage of the fiber with increasing temperature. Reproduced with permission.^[164] Copyright 2002, American Association for the Advancement of Science. b) Schematic illustration of the atrial septal defect prototype after interventional therapy with an occlude. Reproduced with permission.^[177] Copyright 2019, Wiley-VCH. c) I: Schematic illustration of shape memory polymers (SMPs) vascular graft with a diffuser design to minimize the formation of disturbed flow, II: linear-design (control)-like minimization of disturbed flow formation in a diffuser design was visualized in comparison with a direct stepped design through the flow of red fluorescent microbeads in PDMS bioreactors, III: cross-section of haematoxylin and eosin (H&E) on day 18 after grafting of SMPs test tubes. Reproduced with permission.^[173] Copyright 2019, Wiley-VCH. d) A potential application to a ureter stent. Ureter stents were deployed after being placed in the right position with water heating. Reproduced with permission.^[180] Copyright 2009, Wiley-VCH.

studying the controllable drug release behavior and the influence of molecule structure. Theophylline was crosslinked with branched oligo(ϵ -carprolactone) by Nagahama et al.^[179] with theophylline ratios of 10% and 20% being dissolved in hexamethylene diisocyanate and oligoglycerin, respectively. Then, it was cast into a film. After subsequent drying, the drug was loaded in the polymer network chain. The resulting polymer demonstrated biodegradability and shape memory properties. In addition, a rapid temperature-sensitive shape recovery was displayed as temperature increased from 37 °C to 39 °C. Neffe et al.^[180] studied the relationship between shape recovery and drug release process by conducting drug swelling and crosslinking experiments on the same polymer to analyze the difference in drug diffusion and shape recovery (Figure 13d). The result revealed that the crosslinked hydrophilic and hydrophobic drug did not affect the shape recovery; the drug release could be separated from the shape recovery process with minimal invasive implantation, and drug diffusion could be independent of

the biodegradation. Besides, Zainal et al.^[181] demonstrated an SMPs drug release system where drugs and the SMPs component were separate entities. In their study, bulk SMP sealing with a drug reservoir was connected with a Cu resistor heater so that once the external electromagnetic field frequency was tuned to the resonant frequency of the heater, bulk SMP was activated with the drug being released into the environment.

4.3. Flexible Electronics

SMPs-based flexible electronics has become an attractive area of research. SMPs are flexible and can be combined with electronic devices as the substrate. As the temperature reaches T_g , the SMPs substrates are softened to adjust to the rigid electronics. Besides, these metal-free SMPs electronics can maintain stable properties after multiple bending-recovery tests, which is necessary for wearable devices. Yu and co-workers^[182]

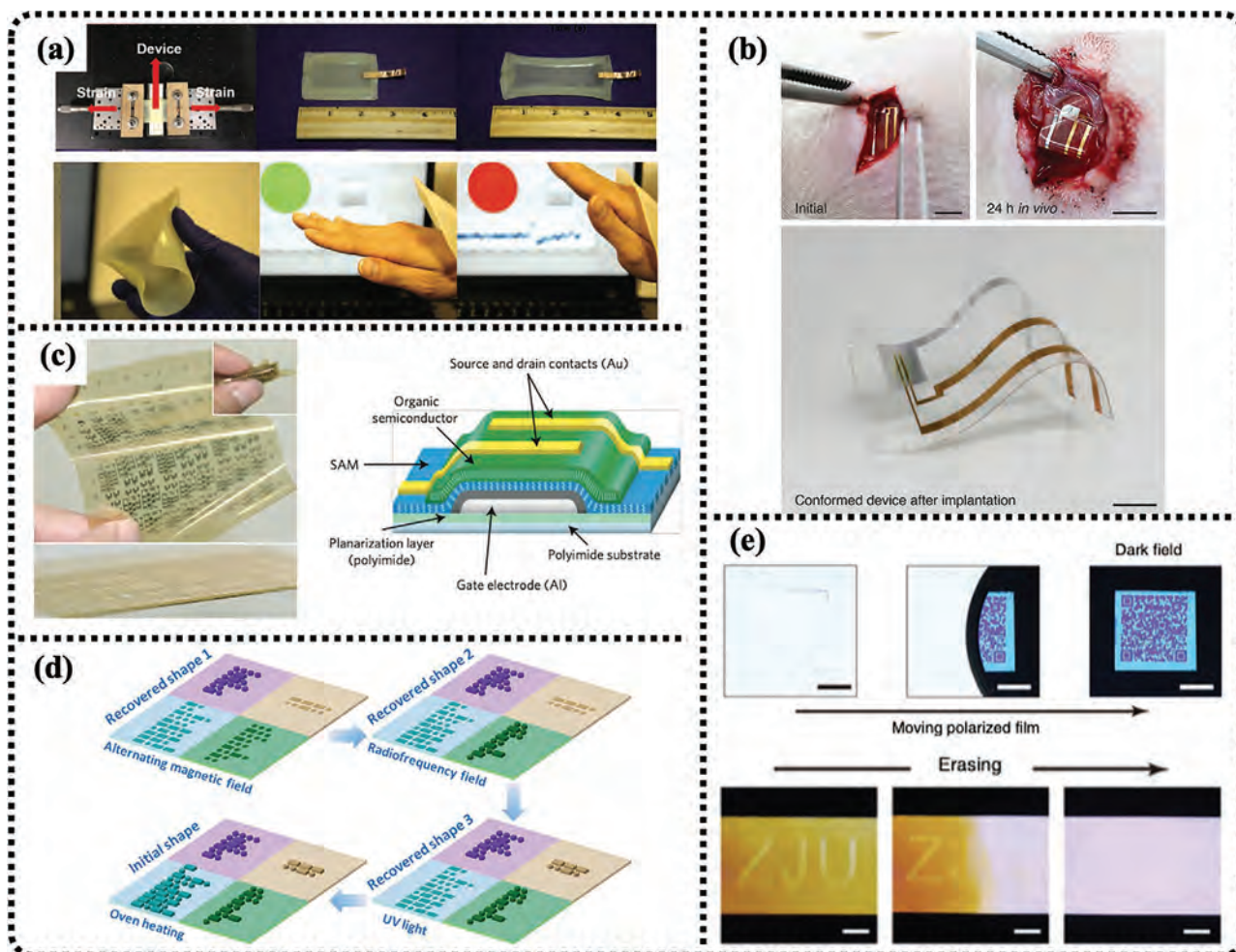


Figure 14. a) Demonstration of the setup for strain testing and shape memory polymer (SMP)-based triboelectric nanogenerators. A smart splint system capable of producing green/red signals under different motion states is presented. Reproduced with permission.^[186] Copyright 2018, Wiley-VCH. b) An organic thin-film transistor coated with SMP conforms to the body tissue of a living rat after being implanted for 24 h. Reproduced with permission.^[188] Copyright 2014, Wiley-VCH. c) Photographs of a 12.5- μm -thick polyimide substrate with functional organic thin-film transistors and organic complementary circuits. The array has an area of 75 \times 75 mm². Reproduced with permission.^[191] Copyright 2010, Springer Nature. d) Step shape recovery process of a shape memory substrate with different Morse codes according to diverse actuation methods. Reproduced with permission.^[194] Copyright 2017, American Chemical Society. e) Stress-induced, mechanically colored images with an invisible quick response code and erasing and rewriting letters. Reproduced under the terms of the CC-BY Creative Commons Attribution 4.0 International license (<https://creativecommons.org/licenses/by/4.0>).^[195] Copyright 2018, The Authors, published by Springer Nature.

fabricated highly flexible silver nanowire electrodes using transparent polyacrylate substrates. A composite with low surface resistance and able to be bent multiple times was used to replace the conventional ITO substrate of a light-emitting diode device. A similar approach was employed to fabricate a CNT/poly(tert-butyl acrylate) (PtBA) composite with a glass transition at a temperature of around 56 °C.^[183] The resulting flexible light-emitting device could be stretched up to 45% linear strain without losing the electroluminescent properties. Adiyani and co-workers^[184] introduced the transduction property of the SMPs into the uncooled IR sensor. A phase transition behavior was connected with IR absorbing, and resonators based on SMPs successfully developed. These resonators were capable of working under the atmospheric pressure and vacuum environment. Furthermore, microelectrode arrays with a 10 \times 10 mm² large area and 126-channel high-density electrodes

were formulated based on shape memory substrates by Wang et al.^[185] These arrays were capable of deforming and unfolding at 37 °C, which was suitable for invasive implantation. Liu and co-workers^[186] developed an SMP-based wearable electronics for harvesting energy and mechanic sense (Figure 14a). Briefly, a conductive liquid was sealed in the polymer shell to build a mini capacitor, which could light 150 green LEDs when being tapped. A smart wrist splint was designed based on shape reprogrammable features to fit human knuckles.

SMPs-based biological electronic devices require completely different materials for medical ones. Biological electronic devices require undegradable and nontoxic materials since they are associated with the human body. As a result, PLA, PU, and PCL are not recommended during the fabrication of these devices. Traditional silicon-based organic electronics are flexible but show poor stability during chronic implantation. However,

thiol-ene/acrylate SMP is the ideal substrate for the fabrication of biological electronic devices. A thiol-ene/acrylate was synthesized by UV light-induced photopolymerization in monomer solution by Ware et al.^[187] The resulting polymer showed a T_g of around 70 °C, although this T_g could be reduced to 37 °C under the plasticization effect in physiological conditions. This temperature, which is close to that of the human body, was suitable for biological use. These properties make the thiol-ene/acrylate polymer suitable for generating implantation devices since it can be inserted in a rigid stage and be softened, ensuring the applicability of the device to tissues. Reeder and co-workers^[188] reported a change of a thiol-ene/acrylate-based organic transistor after implanting it into a living tissue after 24 h (Figure 14b). A thiol-ene/acrylate-based nerve cuff was also reported by Ware et al.^[189] This nerve cuff was capable of recovering the original helix shape in vivo, while external heat was not required during the recovery process, which is essential for a biological device. The nerve cuff was reported to stimulate neural activity, including heart rate and oxygen saturation. Stiller and co-workers^[190] reported an intracortical probe for neural recording and electrochemistry. The generated IC-5-16E device was fully encapsulated in thiol-ene/acrylate polymer, and a 13-week in vivo experiment was performed to assess the chronic intracortical recording and electrochemical stability of the device. In addition to these devices, Sekitani and co-workers^[191] generated a flexible organic transistor (Figure 14c). Here, a pressure sensor array was fabricated on a NIPPON MEKTRON shape memory substrate to detect changes in physical and chemical properties inside long, narrow tubes. Furthermore, Zhang and co-workers^[192] designed twining electrodes based on SMPs for nerve stimulation and recording. Summarily, a conductive mesh layer was indented on the SMP substrate, followed by shape twisting at 37 °C on the vagus nerve. Self-climbing behavior occurred as the twined electrode was reheated at body temperature.

The aforementioned methods focus on the use of SMPs as a substrate for the encapsulation of electronic devices, or as sensors to detect external changes under chemical or physical stimuli. SMPs can also work as information carriers, without additional electronic elements. Pretsch and co-workers^[193] reported an SMP-based QR code with poly(ester urethane) and epoxy as the primary material. Here, the authors reported the use of CO₂-laser ablation technique to engrave QR codes onto the polymer surface. The resulting QR code was capable of elongating up to 100% for multiple cycles and working as an information carrier. Li and co-workers^[194] combined different Morse codes in one epoxy-based SMPC (Figure 14d). The epoxy substrate was divided into four separate areas containing Fe₃O₄, CNT, p-aminodiphenylimide, and neat epoxy polymer. Each Morse code had its corresponding embossed area, and the stimulus under UV light, electromagnetic, and radiofrequency fields activated the corresponding areas according to the embedded material. At a macro scale, Zhang and co-workers^[195] manipulated the complex stress distribution in different SMP films using an inkjet printer. The partial plasticity control by digital grayscale photothermal effect resulted in stress-induced mechanically colored images, while invisible stress converted to visible mechanical color under polarized light (Figure 14e). The SMPs endow electronics with further functionality and

make them capable of working in different environments with a more straightforward preparation step compared to conventional electronics.

4.4. Soft Robotics

Robots are designed to imitate human behavior and extend human capability limits. Traditional robots are usually bulk, heavy, rigid, and not capable of interactions with humans. A variety of novel materials have been discovered, promoting the development of soft robotics and bringing new possibilities in solving problems that could, otherwise, not be addressed by conventional rigid robots. These soft robots are made of complex elastomers and polymers, characterized by lightweight, low cost, high flexibility, and mechanic compliance. Until now, a variety of soft robots, including gripper, actuator, crawling robot, and other complex ones, have been developed based on inflexible SMPCs. These robots have great potential to complete complex tasks, such as drug delivery, search and rescue, and acting as human assistants.

LCEs are considered promising smart active materials for the fabrication of soft robots due to their flexibility and reversible shape memory. Generally, these robots consist of thin LCE films combined with electric or magnetic segments. Xiao and co-workers^[69] fabricated different electrically powered LCE structures including gripper, crawling machine, and walking robots by laminating LCE films with flexible Kapton and embedding a resistive wire in between them. Complex shape morphing was demonstrated due to the different programmed 3D LCE structure. For the photo-activated crawling soft robot, switching of the localized light onto the photosensitive polymer substrate helped realize the reversible bending of the robot to produce locomotion. A bilayer soft inchworm robot consisting of LCE membranes and PE substrates was developed by Yamada et al.^[196] The robot motion induced by switching of UV and visible light was also characterized. A photo-sensing artificial muscle consisting of carbon black-filled LCEs was developed by Wang et al.^[197] The soft robot was capable of autonomous sensing and locomotion under light and heat stimulation. Rogoż and co-workers^[63] fabricated a light-driven caterpillar soft robot, in which a single LCE film with controlled photo-induced polymerization was synthesized as the main body. The changing of the laser excitation state enabled reversible localized shape deformation, resulting in crawling, climbing, and squeezing. LCEs are suitable for artificial muscles because they have similar performance to human muscles. However, this also limits their use in high-intensity applications since LCEs generally have poor mechanical properties. Recently, soft robots based on reversible semicrystalline polymers were reported. For instance, Xu and co-workers^[198] incorporated CNTs in a poly(ethylene-co-octene) matrix to fabricate a walking robot that could be driven with a low voltage (≤ 36 V) or IR light irradiation. Yang and co-workers^[199] synthesized *cis*-1,4-polybutadiene-PE copolymer and used it to develop a semicrystalline polymer-based walking robot (Figure 15a). IR light penetration into the polymer resulted in localized segment contraction and made the light-driven soft robot walker accessible.

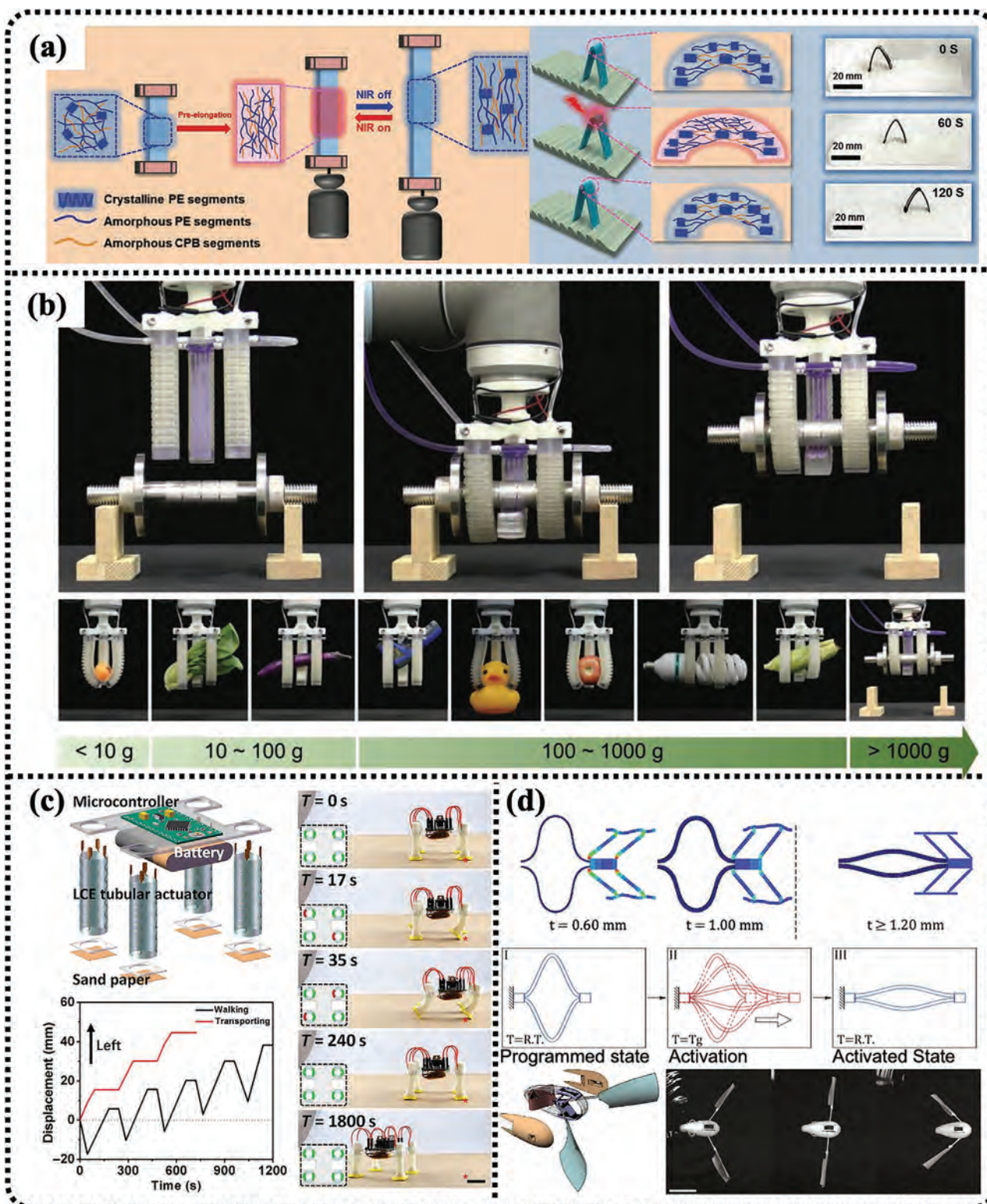


Figure 15. a) Schematic illustration of a light-driven walker upon turning on and off near infrared (NIR) light. Reproduced with permission.^[199] Copyright 2019, Wiley-VCH. b) Demonstration of high load capacity and good shape adaptivity by a versatile gripper equipped with three fast-response and stiffness-tunable actuators. Reproduced with permission.^[201] Copyright 2019, Wiley-VCH. c) Schematic of the robot, which is mainly composed of a microcontroller, battery, and four liquid crystalline elastomer (LCE) tubular actuators. Reproduced with permission.^[205] Copyright 2019, The Authors, published by American Association for the Advancement of Science (AAAS). Reprinted/adapted from ref. [205] © The Authors, some rights reserved; exclusive licensee American Association for the Advancement of Science. Distributed under a Creative Commons Attribution NonCommercial License 4.0 (CC BY-NC) <http://creativecommons.org/licenses/by-nc/4.0/>. d) Illustration of finite-element simulations and propulsion of bistable shape memory polymer (SMP) muscle in hot water. Reproduced with permission.^[207] Copyright 2018, published by National Academy of Sciences.

Shape memory gripper is a simple soft robot that can produce gripping and lifting actions. It only requires programmed bending and recovery behavior from the polymers, making it easy to be built by a variety of SMPCs with desired mechanical properties. Wei and co-workers^[200] built an electroactive hybrid gripper based on direct 3D printing. Printable PLA/CNT/Ag ink with high electricity ($>2.1 \times 10^5 \text{ S m}^{-1}$) made the gripper capable of producing rapid responses at different voltages. Zhang and co-workers^[201] embedded SMPC layers into a 3D-printed pneumatic soft actuator when designing a fast response gripper (Figure 15b). The stiffness-tunable robotic gripper could lift objects weighing between 10 g and 1.5 kg within 32 s. In addition, a mini multimaterial gripper fabricated by 4D printing technology was demonstrated by Ge et al.^[202] It could lift a screw upon shape deforming. Compared to one-way shape memory, a two-way shape system is preferred in soft robots owing to the necessity of repeatable actions. A reversible shape memory gripper developed by McCoul and co-workers^[203] consists of conductive SMPC electrodes with three independently controlled segments and is capable of lifting a load of more than 30 g at 300 V. Jin and co-workers^[60] used the origami technology to fabricate a variety of soft robots by incorporating esters and cinnamates into the crystalline PU network. The crosslinked structure was stretched with UV irradiation to increase network anisotropy, which is crucial for creating a reversible SMP. Consequently, different origami uni-bots capable of transforming their shapes between 0 °C and 80 °C were successfully created. Moreover, a magnetic and photo-controlled grabber was developed by Liu and co-workers^[204] in which simultaneous magnetic actuation and photothermal heating realized reconfigurable soft robots based on SMPCs.

The soft robot that could produce complex motion states was demonstrated by He et al.^[205] Tubular LCE embedded with heating wire was designed to produce multidirectional movement. Through the introduction of a microcontroller to the LCE actuator, a multimodal soft robot capable of remote control was created (Figure 15c). A bistable shape memory actuator was reported by Chen and co-workers^[206] and designed with activation and load-bearing capability to operate as the basic unit for driving robot motion. During further research, a swimming robot with the bistable shape memory muscle was designed,^[207] which could produce sequential and directional propulsions upon different shape programming procedures according to changes in the surrounding water temperatures (Figure 15d). The autonomous cargo-delivery capability was also demonstrated as the swimming robot navigated back and forth to the deployment point.

4.5. Shape Memory Arrays

Shape memory arrays that consist of repeat units such as cylinders, cuboids, prisms, cones, and polyhedral can be fabricated by silica molding, nanoindentation, or localized laser^[208] (Figure 16a). Altering the arrangement and intervals of the repeat SMP units will significantly affect SMP topography. Recently, research efforts have focused on wettability and control of adhesiveness in SMP substrates by the controllable shape memory array. For example, Chen and co-workers^[209,210]

investigated the wettability of SMP pillar arrays made by epoxy resin and found changes as the pillar structure turned from tilt to flatten upon shape transition. Meanwhile, Cheng and co-workers^[211] achieved control of droplet motion on a hydrophobic surface by controlling the shape of SMP pillars at a microscale level. This was done by the creation of a repeatable switch between superhydrophobic isotropic and anisotropic SMP pillar arrays. The tilt angle was a critical factor in realizing this behavior. In addition to controlling the water droplet movement, Lv and co-workers^[212] fabricated an SMP pillar array with tunable adhesive superhydrophobicity (Figure 16b). They found that when the space between the pillars was greater than 20 μm, the SMP arrays showed low adhesion superhydrophobicity, while a high adhesion superhydrophobicity was achieved when a pit pillar configuration was applied.

The wrinkled surfaces can be fabricated by pressure indentations on the SMP surfaces above the transition temperature with prestretching of the SMP, followed by a coating of the surface metal as the SMP returns to the original shape below a specific temperature. Then the metal contracts and forms a wrinkled structure. When the wavelength of these wrinkles is on the macro scale, structural color exhibits on the surface of the material^[213] (Figure 16c). Zhao and co-workers^[214] investigated the structural color of different wrinkle patterns on SMP surfaces by coating a 10 nm gold layer onto the polyurethane surface through sputter deposition. The result showed that the degree of wrinkles strongly depended on the properties of the thin gold layer and the SMPs substrate, which created different wrinkle patterns (Figure 16d). Ebara and co-workers^[215] extended the wrinkle wavelength to the nanoscale, which created a wrinkle pattern that became transparent at human body temperature (Figure 16e). Yang and workers^[216] studied the photonic shape memory behavior on a liquid crystalline blue-phase film by self-assembling a liquid crystal mixture into the periodic structure followed by UV light crosslinking. Red, green, and blue colors that corresponded to different levels of periodicity were displayed. These reflection colors could be altered and recovered with thermo-induced indentation and shape recovery process.

Light reflection can be tuned by the application of shape memory arrays in SMPs as well. Porous surface structures can be fabricated by silica templating, and the thickness of the porous layer, as well as pore diameter, is expected to affect refraction and reflection of light. With the control of structure-deformation behavior, the color of SMPs porous surfaces can be changed under different shape stimuli. For instance, Espinha and co-workers^[217] fabricated an SMP porous membrane that changed transparency under deformation as samples narrowed in the direction orthogonal to the stretching axis during elongation. Fang and co-workers^[218] investigated rewritable photonic patterns based on shape memory inverse opals by fabricating a porous multilayer structure with a diameter of approximately 200–400 nm. Different micropatterns were written onto the SMP copolymer membrane with a 1 mm diameter spherical sapphire tip, while a combination of photonic crystal array and SMPs made different optic devices available. Wu and co-workers^[219] incorporated monodisperse nanoparticles in a poly(ethylene terephthalate) (PET) film with stepwise emulsion polymerization. The core–interlayer–shell nanoparticles were

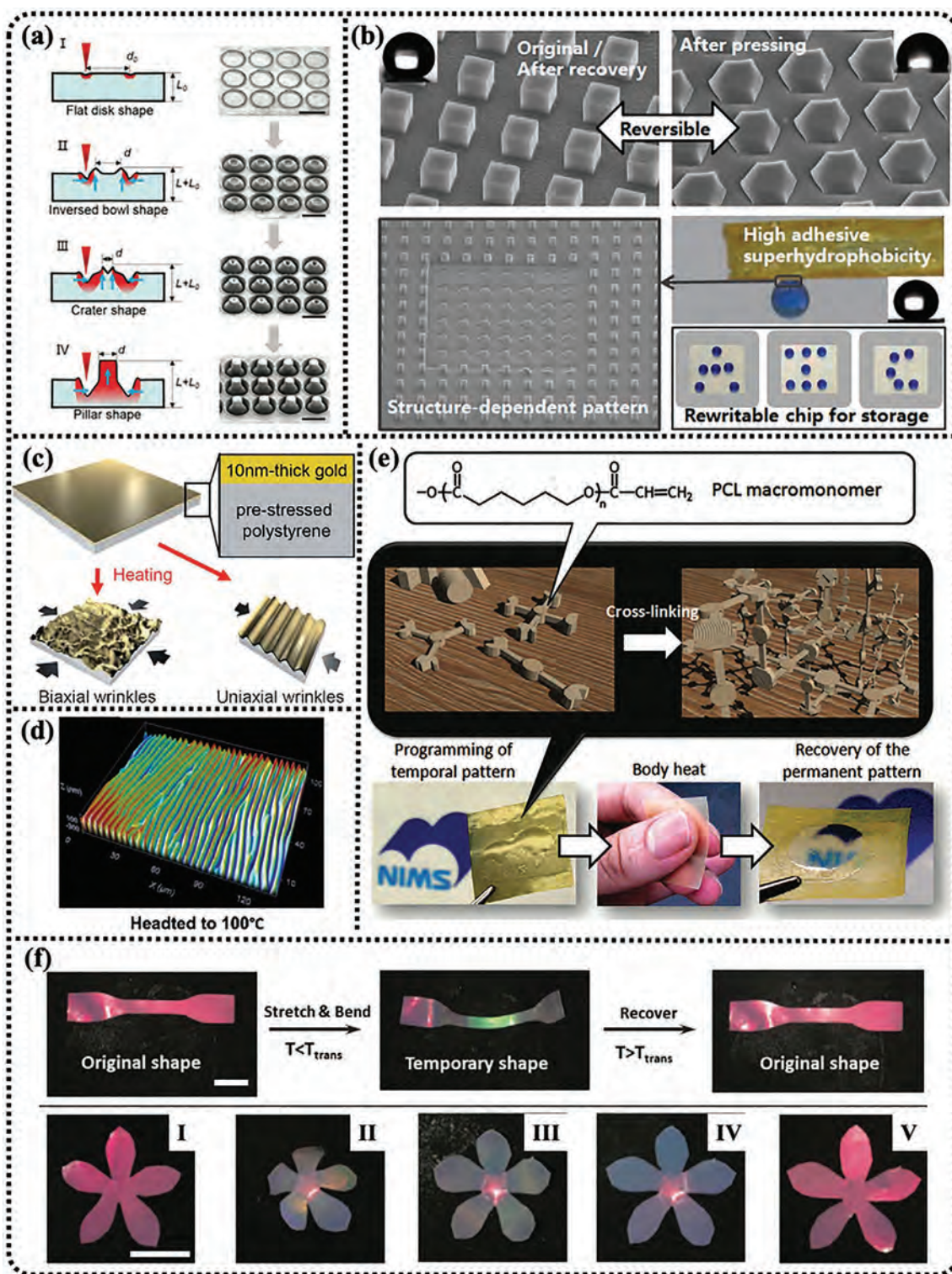


Figure 16. a) Shrinkage-growth model of laser-induced self-growing micropillars, I–IV: the schematics of the cross-sectional profile of microstructure and corresponding scanning electron microscopy (SEM) images. Reproduced with permission.^[208] Copyright 2018, Wiley-VCH. b) Shape memory array substrate as a rewritable platform for a droplet storage chip. Reproduced with permission.^[212] Copyright 2016, American Chemical Society. c) Scheme of fabrication of biaxial and uniaxial wrinkles. Reproduced with permission.^[213] Copyright 2009, Wiley-VCH. d) Surface morphology of uniaxial wrinkles. Reproduced with permission.^[214] Copyright 2011, IOP Publishing Ltd. e) Schematic illustration of shape memory films with a rewritable surface on demand by body heat based on utilizing crosslinked poly(ϵ -caprolactone) (PCL). Reproduced with permission.^[215] Copyright 2011, Wiley-VCH. f) Thermochromic shape memory effects of the red shape memory composite film. The scale bar is 1 cm, I–V: the illustration of the shape recovery process of red film heated above T_{trans} . Reproduced with permission.^[219] Copyright 2019, Royal Society of Chemistry.

well dispersed in the PET matrix to form photonic crystals. The reflection color of the photonic crystals/PET composite was tunable during the shape programming, and recovery process as the strain changed the lattice spacing (Figure 16f). Xie and co-workers^[220] designed an ink-free rewritable paper based on ferroferric oxide-carbon core-shell nanoparticle-based photonic crystal and photocurable acrylate polymer. The reflection color was switchable under electric field actuation.

4.6. 4D Printing

The technology of 4D printing refers to a novel additive manufacturing process with an extra time dimension compared to traditional 3D printing.^[221] Generally, 3D printing is an additive manufacturing process associated with the digital model. Differently, 4D printing entails 3D-printed components capable of shifting from one structure to another with time. The process of 3D and 4D printing is, therefore, identical and involves fused deposition modeling (FDM), stereolithography apparatus (SLA), and direct ink writing. The critical factor that enables the transformation of printed components is the material. The technology of 4D printing can be accessible by the application of SMPs in 3D printing technology. The printed SMPs can alter their shape by interacting with external stimuli. In fact, 4D printing combines the advantages of 3D printing and SMPs. Complex SMPC structures can be designed and manufactured in a relatively short period, which is important for making custom tools for biomedical devices, aerospace engineering, and soft robotics.

Research in 4D-printed SMPs has focused on the synthesis of raw materials, microstructures, printing, and controllable morphology^[222] (Figure 17a). For instance, Mao and co-workers^[223] fabricated a two-way reversible actuator with a multilayer structure consisting of SMPs, elastomer, and hydrogels, and designed a printed ladder that could switch into a bench. Because of the multilayer structure, the transformation process without shape programming became possible. A high-resolution 4D printing technology was studied by Ge and co-workers^[202] by applying a photocurable methacrylate precursor to form complex printed microstructures of up to 1 μm (Figure 17b). This allowed the printing of a variety of SMPs with controllable thermal stimulus. Zhang and co-workers^[224] prepared a variety of PLA circular-braided tubes using the FDM technology, and further characterized the influence of braided microstructure on shape memory. They also demonstrated that a braided PLA/silicone elastomer matrix could enhance the recovery force and ratio. Wei et al.^[225] demonstrated the direct writing of photoresponsive PLA-based ink. The polymer ink was incorporated with Fe_3O_4 , showing great potential for the self-expandable intravascular stent (Figure 17c). Furthermore, Huang and co-workers^[226] reported an ultrafast 4D SLA technology based on digital control of stress on a 2D membrane (Figure 17d). An acrylate copolymer precursor was filled between two glass slides and a specific area was exposed to visible light with different periods corresponding to the diversity in crosslinking. The printed 2D film could swell into 3D structures by careful design of the exposure parameters in the precursor. This concept of 2D to 3D transformation was also

adopted by Zhang and co-workers^[227] who obtained a variety of 3D structures through the printing procedure. Potential applications of nanophotonic devices and wearable devices were also demonstrated. Deng et al.^[228] reported an open-air 4D printing system with an SLA technique. Thermoset resin was replaced by thermoplastic 4-acryloylmorpholine polymer resin during the printing procedure at a high printing speed. Meanwhile, the 4-acryloylmorpholine polymer demonstrated shape memory property at 80 °C and recyclability in water (Figure 17e).

The technology of 4D printing has great potential for connecting with other research areas. Currently, a variety of 4D-printed scaffolds are applied to biomedical devices. For instance, Miao and co-workers^[229] fabricated a 4D bioscaffold with soybean oil epoxidized acrylate by stereolithography. The scaffold was capable of producing a shape recovery transition. Renewable crosslinked vegetable oil has excellent biocompatibility and can further be developed into medical devices. In addition, Liu and co-workers^[230] printed the active PNIPAM and nonactive polyacrylamide based on direct ink writing and they successfully transformed the complex shape through the active/nonactive material distribution area in the 3D tubular structure. These tubular structures were utilized in vascular stents. A porous PLA scaffold constructed by FDM printing and incorporated with bioresorbable hydroxyapatite (HA) nanoparticles was reported by Senatov et al.^[231] The HA particles worked as centers for rigid phase formation, which impacted shape recovery stress and ratio. Analysis of mesenchymal stromal cell colonization demonstrated the adhesive properties of the PLA/HA porous scaffold and its potential in medical applications. Moreover, Zhang and co-workers used 4D printing to fabricate a composite structure consisting of PLA and Fe_3O_4 nanoparticles for bone repair.^[232] Here, the shape recovery process could be triggered at 275 kHz. This method was also applied by Zhao and co-workers,^[233] who designed and fabricated a tracheal stent that could be implanted in the body to recover its original shape under a magnetic field.

4.7. Dry Adhesion

As a fast-growing innovative technology, numerous innovative SMP dry adhesive systems have been explored to develop soft grippers.^[234-237] The conventional wet adhesive systems comprising multicomponent with glue are not reusable. As a consequence, they cannot be used to grasp and drop an object.^[238] To solve these issues, a dry adhesive SMP system with enough adhesive strength and reusability was employed. In the dry adhesion process, the SMPs were softened and sticky when heated, and they came into close contact with different types of objects under pressure. Objects would be stuck to the SMP surface after cooling primarily by van der Waals adhesive forces and released with localized heating. Xie and Xiao^[239] developed a self-peeling reversible dry adhesive (SPRA) system to mimic gecko's adhesion mechanism. The SPRA system was composed of bilayer SMP structures with thermoset elastomer and fabricated through a two-step curing procedure. The pull-off strength reached about 60 N cm^{-2} with reversal adhesion. The nonpatterned dry adhesion behavior was analyzed by Wang and co-workers.^[240] In further research, the microscopic array structure was employed to improve the adhesiveness for the compliant

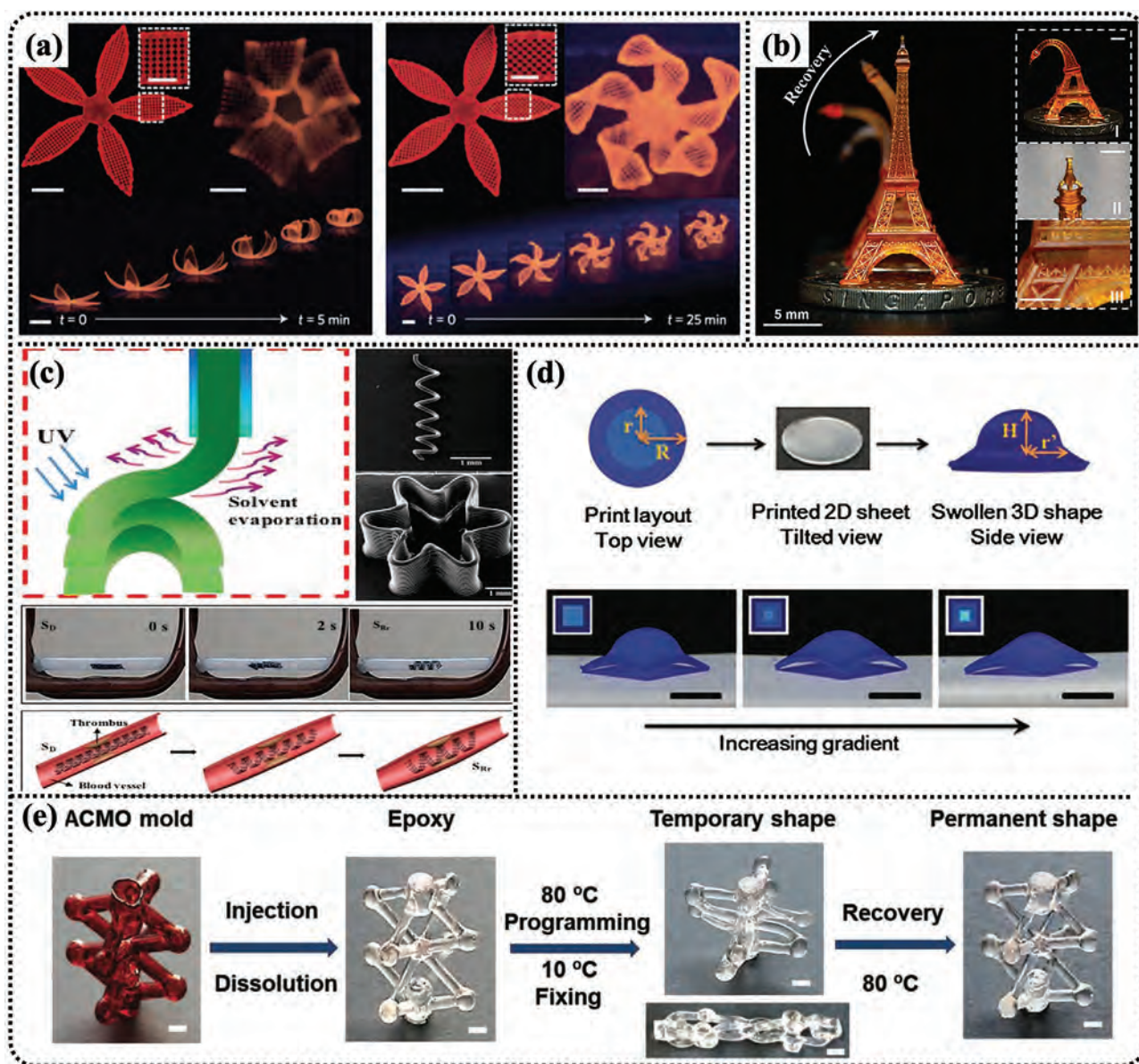


Figure 17. a) Complex flower morphologies generated by biomimetic 4D printing. Reproduced with permission.^[222] Copyright 2016, Springer Nature. b) 4D-printed shape memory Eiffel tower. Reproduced under the terms of the CC-BY Creative Commons Attribution 4.0 International license.^[202] Copyright 2016, The Authors, published by Springer Nature. c) Schematic illustration of the direct ink writing of active shape-changing architecture that can be actuated under a magnetic field. Reproduced with permission.^[225] Copyright 2017, American Chemical Society. d) Process illustration from a planar sheet with patterned concentric circles swollen into a cap-shape 3D structure and cap geometries controlled by crosslinking density distribution. Reproduced with permission.^[226] Copyright 2016, Wiley-VCH. e) Construction of an epoxy SMP structure. Reproduced with permission.^[228] Copyright 2019, Wiley-VCH.

materials. Eisenhaure and co-workers^[241] presented an SMP substrate with repeatable microtips (Figure 18a). The SMP surface demonstrated great reversible dry adhesion performance to the glass substrate (>18 atm). Tan and co-workers^[242] studied the adhesion capability of graphene-reinforced SMP pillar array on rough surfaces. SMP micropillar array incorporated with graphene capable of switching its adhesion stress at the detaching interface under light, heat, or electric stimulus was developed. In addition, Chen and co-workers^[243] studied the interlocking behavior between tangled SMP pillar arrays. The unique pillar to pillar structure raised adhesion force about $53.6 \pm 2.1 \text{ N cm}^{-2}$

in the normal direction and $71.9 \pm 23.2 \text{ N cm}^{-2}$ in the shear direction compared to the pillar to flat configuration.

In particular, there has been growing interest in the application of controllable dry adhesion for microdevices, especially for the integration of electronic devices' transfer.^[244] Huang and co-workers^[245] incorporated localized laser pulse with micropatterned SMP stamps to improve the transfer printing process (Figure 18b). The laser beam enabled SMP stamps to pick and drop microdevices under selective heating. As a result, Si squares and Si ribbons (thickness: 200 nm) were transferred onto a PDMS substrate without damage. In another research,

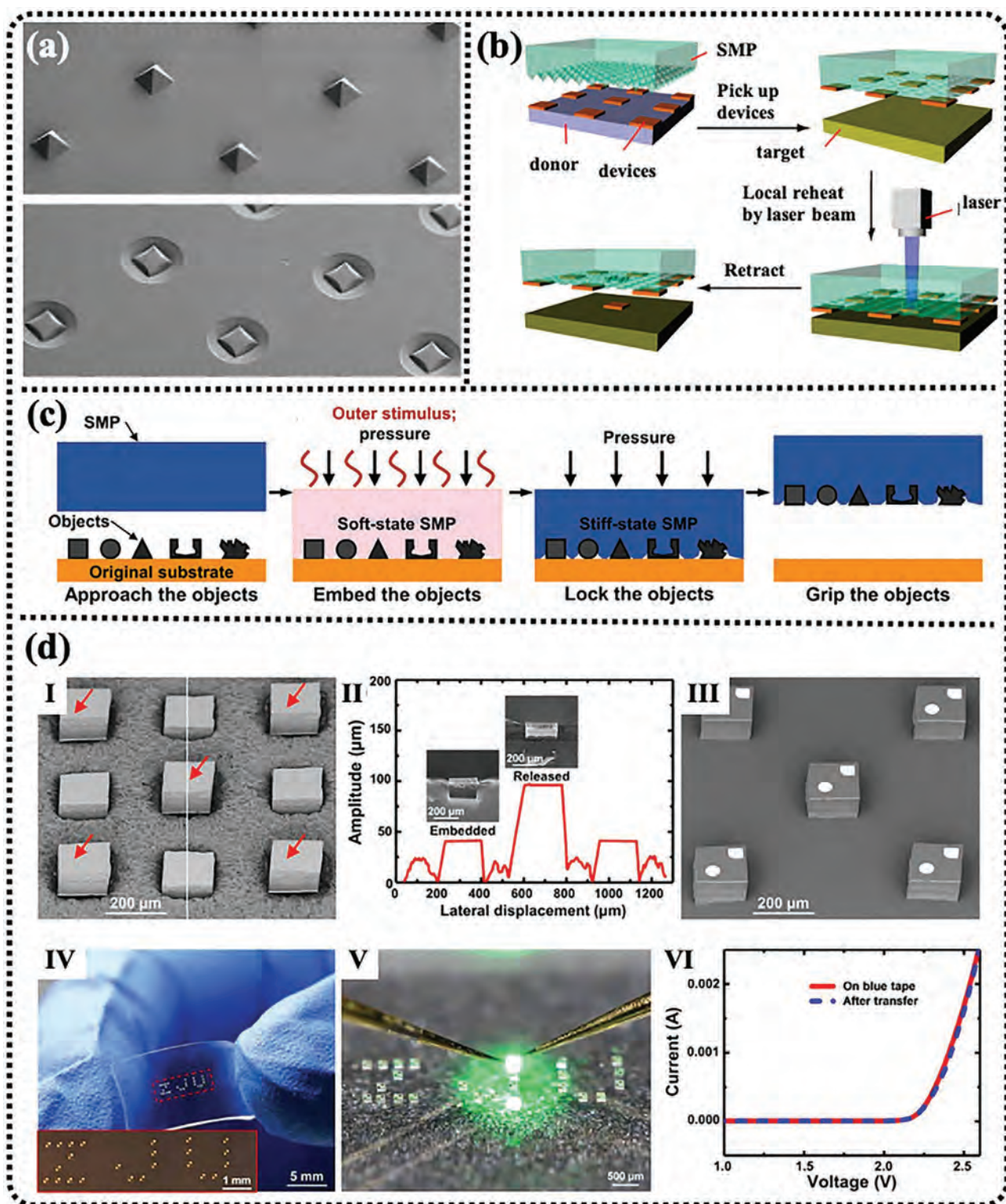


Figure 18. a) SEM image of SMP surface in the permanent state and temporary state. Reproduced with permission.^[241] Copyright 2013, American Chemical Society. b) Scheme of transfer printing process via localized laser beam. Reproduced with permission.^[245] Copyright 2016, American Chemical Society. c) Scheme for the gripping process of the universal SMP gripper and d) transfer printing of planar micro light-emitting diode (LED) chips. I: SEM images of the universal SMP microgripper, II: cross-section profile for universal SMP microgripper, III: the selectively printed LED chips on the surface of PDMS, IV: patterned printing of micro-LED chips, V: micro-LED chips powered on the probe station, VI: voltage-current curve of micro-LED chips before and after transfer printing. Reproduced with permission.^[247] Copyright 2020, The Authors, published by American Association for the Advancement of Science (AAAS). Reprinted/adapted from ref. [247] © The Authors, some rights reserved; exclusive licensee American Association for the Advancement of Science. Distributed under a Creative Commons Attribution NonCommercial License 4.0 (CC BY-NC) <http://creativecommons.org/licenses/by-nc/4.0/>.

the SMP stamp system was capable of assembling the solid microscale building blocks into 2D or 3D configuration.^[246] A micromotor with a rotatable rotor was designed to demonstrate the capability of creating new microelectromechanical system devices with more sophisticated structures. More recently, a universal SMP gripper was developed by Linghu and co-workers^[247] with the simplest block structure (Figure 18c). This versatile gripper was applicable to multiscale objects with diverse sizes and arbitrary shapes, which would increase the reliability of transfer printing (Figure 18d). The gripping force mainly derives from the interlocking and friction effects, which requires additional mechanic analysis.

4.8. Self-healing

Self-healing has been extensively studied in biology and material science over the years. The combination of self-healing property and materials will significantly reduce the maintenance cost and service life of the appliances. Conventionally, a capsule with healing precursors is embedded inside the material so that when a crack damages the interior of the material, the precursor is released from the capsule, polymerized by a catalyst, and dispersed in material matrix. The polymerization reaction, therefore, fixes the damaged area.

The self-healing procedure for a thermoplastic polymer involves heating the composite above the transition temperature of the thermoplastic polymer. This enables the polymer to flow into the crack due to the thermoplastic polymer's flow-ability at high temperatures. As the temperature reduces, the thermoplastic polymer is fixed, and the composite is healed. Since not all the recognized thermoplastic polymers have shape memory effect, the self-healing process of the thermoplastic polymer cannot be applied to the self-healing process of the SMPs. Instead, the self-healing of SMPCs has been demonstrated to be the synergy of shape memory effect and thermoplastic polymer fluidity. The self-healing process was demonstrated by Li and co-workers^[248,249] with the SMPs as a matrix and the thermoplastic polymer as filler. Before self-healing, polymer composite should be compressed during the shape programming process. Moreover, when damage reoccurs after the cooling process, reheating the polymer composite narrows the crack opening under the storage stress. Finally, as the polymer composite is heated above the transition temperature of the thermoplastic particles, the crack is filled and healed. During this process, the shape memory effect, in conjunction with the thermoplastic particles, heals the crack. SMP fibers can be utilized as well. For instance, Hu et al.^[250] reported spider silk-like SMP fiber that could be used for the self-healing process. The fiber was programmed with a cold drawing process, which, unlike in the case of the SMPs as self-healing matrix, did not need external confinement.

4.9. Smart Textiles

Textiles have hundreds of years of history in research and development. Smart textiles refer to a combination of smart materials and conventional textiles in recent decades, which result in self-cleaning, moisture control, and self-shape adaptation

to textiles.^[251] The more complex functionalities in smart textiles necessitate the application of novel materials. At the filament level, the fiber possesses a higher stress response compared to that in the films, making it applicable to wearable clothes.^[252] Smart polymer textile was also studied by Chen and co-workers^[253] who synthesized a moisture-sensitive shape memory PU fiber. A pyridine ring incorporated into the polymer network as the moisture absorption unit showed that the temperature and relative humidity influenced moisture absorption. Hu et al.^[98] incorporated cellulose nanowhiskers into the PU network, with both temperature and water applied to trigger shape recovery of the copolymer. Chen and co-workers^[254] designed a smart orthopedic system that was expected to drop foot therapy. Here, a conductive acrylate-based copolymer was fabricated with silver coating nylon yarns by full Milano stitching. Tunable shape memory ankle-foot orthoses assisted in ankle motions with 10 V actuation.

5. Summary and Outlook

Tremendous progress has been made in the multifunctionality and performance of SMPs since the 1960s, and both the commercial and advanced applications have rapidly emerged with the improvement in the understanding of shape memory behavior. In this review, the conventional one-way, two-way, and multiple SMPs were demonstrated in terms of the potential benefit to exploit shape memory effects in a variety of novel polymers. In particular, specific attention was paid to the shape memory behavior based on the exchangeable molecule bond and athermal stimulus methods. The thermomechanical theory disclosed the underlying mechanism to design SMPs with reversible molecule switches compared with irreversible chemical reactions. Novel synthesis and fabrication technologies have greatly expanded the research on multifunctional SMPs. For instance, the conductive SMPs with enhanced mechanical performance can be used to construct aerospace equipment and soft robotics. The water- and pH-sensitive SMPs offer a sea of opportunities to improve the drug delivery system. Besides, notable remote actuation technologies have dramatically expanded the application range of SMPs, especially for the shape memory arrays and flexible electronics since localized shape memory behavior can be triggered with the optimized magnetic field or luminous radiation under a microscopic scale. Throughout the whole review, we speculate that the discovery of the shape memory mechanism could accelerate the enhancement in SMP performance. The polymer reinforcement and multifunctionality are interdependent to meet real-world applications.

For future research, we anticipate that several challenges related to the following areas need to be addressed. First, special attention should be paid to the synthesis and reinforcement of two-way SMPs. Despite the use of one-way shape memory effect in some applications, two-way shape memory behavior is preferred in the future due to high applicability in fields such as soft robotics and flexible electronics. The reinforced two-way SMPs have the potential to show recovery stress comparable to the shape memory alloy. Second, the precise control technology of shape recovery behavior is another exciting topic. With

numerous research activities currently focusing on the beginning and termination of the shape memory process, the intermediate shape during the recovery process has been ignored. By achieving the precise control of intermediate shapes, we could develop multiple SMPs with a single transition phase. This may open up many new SMPs applications. Furthermore, the new discovery of shape memory effect would spring up during the polymer synthesis process. For example, a reversible SMP that could contract upon heating, maintain the contracted structure during cooling without external stress, and recover when reheated may exist. Moreover, the research on nonreversible and athermal chemical reactions can help explore a new shape memory phenomenon.

We expect these challenges and opportunities could be addressed to produce further innovative products. SMPs and their corresponding effects have become increasingly familiar to material scientists, owing to the broad research interest they have attracted. It is believed that SMPs with better functionality and portability would emerge in the future. The use of controllable and deformable SMPs would lead to a new generation of soft stimuli-responsive materials to resolve scientific challenges.

Acknowledgements

This work was funded by the National Natural Science Foundation of China (Grant Nos. 11632005 and 11672086).

Conflict of Interest

The authors declare no conflict of interest.

Keywords

actuation, polymer composites, shape memory polymers, stimuli-responsive materials

Received: January 31, 2020

Revised: May 18, 2020

Published online: September 23, 2020

- [1] X. Zhang, L. Chen, K. H. Lim, S. Gonuguntla, K. W. Lim, D. Pranantyo, W. P. Yong, W. J. T. Yam, Z. Low, W. J. Teo, H. P. Nien, Q. W. Loh, S. Soh, *Adv. Mater.* **2019**, *31*, 1804540.
- [2] Y. Forterre, J. M. Skotheim, J. Dumais, L. Mahadevan, *Nature* **2005**, *433*, 421.
- [3] A. Charlesby, in *Atomic Radiation and Polymers*, Vol. 1 (Ed: A. Charlesby), Pergamon, Oxford, UK **1960**, 198.
- [4] G. Odian, B. S. Bernstein, *J. Appl. Polym. Sci.* **1964**, *8*, 1853.
- [5] A. Charlesby, L. Novaković, O. Gal, *Int. J. Radiat. Appl. Instrum. C. Radiat. Phys. Chem.* **1987**, *30*, 67.
- [6] L. Peponi, I. Navarro-Baena, A. Sonseca, E. Gimenez, A. Marcos-Fernandez, J. M. Kenny, *Eur. Polym. J.* **2013**, *49*, 893.
- [7] P. Miaudet, A. Derré, M. Maugey, C. Zakri, P. M. Piccione, R. Inoubli, P. Poulin, *Science* **2007**, *318*, 1294.
- [8] T. Chung, A. Romo-Uribe, P. T. Mather, *Macromolecules* **2008**, *41*, 184.
- [9] J. Li, W. R. Rodgers, T. Xie, *Polymer* **2011**, *52*, 5320.
- [10] L. Yu, H. Shahsavan, G. Rivers, C. Zhang, P. Si, B. Zhao, *Adv. Funct. Mater.* **2018**, *28*, 1802809.
- [11] G. J. Berg, M. K. McBride, C. Wang, C. N. Bowman, *Polymer* **2014**, *55*, 5849.
- [12] Q. Zhao, H. J. Qi, T. Xie, *Prog. Polym. Sci.* **2015**, *49-50*, 79.
- [13] Y. Liu, H. Du, L. Liu, J. Leng, *Smart Mater. Struct.* **2014**, *23*, 023001.
- [14] A. Lendlein, M. Behl, B. Hiebl, C. Wischke, *Expert Rev. Med. Devices* **2010**, *7*, 357.
- [15] I. S. Kolesov, H. J. Radosch, *eXPRESS Polym. Lett.* **2008**, *2*, 461.
- [16] W. Liu, H. Chen, M. Ge, Q.-Q. Ni, Q. Gao, *Mater. Des.* **2018**, *143*, 196.
- [17] M. Y. Razaq, M. Behl, U. Nöchel, A. Lendlein, *Polymer* **2014**, *55*, 5953.
- [18] K. M. Lee, H. Koerner, R. A. Vaia, T. J. Bunning, T. J. White, *Soft Matter* **2011**, *7*, 4318.
- [19] Y. Liu, Y. Li, H. Chen, G. Yang, X. Zheng, S. Zhou, *Carbohydr. Polym.* **2014**, *104*, 101.
- [20] A. Lendlein, O. E. C. Gould, *Nat. Rev. Mater.* **2019**, *4*, 116.
- [21] H. Tobushi, K. Okumura, S. Hayashi, N. Ito, *Mech. Mater.* **2001**, *33*, 545.
- [22] J. Gu, J. Leng, H. Sun, *Mech. Mater.* **2017**, *111*, 1.
- [23] T. D. Nguyen, H. Jerry Qi, F. Castro, K. N. Long, *J. Mech. Phys. Solids* **2008**, *56*, 2792.
- [24] C. P. Buckley, D. C. Jones, *Polymer* **1995**, *36*, 3301.
- [25] H. Tobushi, T. Hashimoto, S. Hayashi, E. Yamada, *J. Intell. Mater. Syst. Struct.* **1997**, *8*, 711.
- [26] Y. Liu, K. Gall, M. L. Dunn, A. R. Greenberg, J. Diani, *Int. J. Plast.* **2006**, *22*, 279.
- [27] Y.-C. Chen, D. C. Lagoudas, *J. Mech. Phys. Solids* **2008**, *56*, 1752.
- [28] Y.-C. Chen, D. C. Lagoudas, *J. Mech. Phys. Solids* **2008**, *56*, 1766.
- [29] K. Yu, H. J. Qi, *Soft Matter* **2014**, *10*, 9423.
- [30] H. Park, P. Harrison, Z. Guo, M.-G. Lee, W.-R. Yu, *Mech. Mater.* **2016**, *93*, 43.
- [31] Y. Li, Z. Liu, *Polymer* **2018**, *143*, 298.
- [32] H. J. Qi, T. D. Nguyen, F. Castro, C. M. Yakacki, R. Shandas, *J. Mech. Phys. Solids* **2008**, *56*, 1730.
- [33] X. Guo, L. Liu, B. Zhou, Y. Liu, J. Leng, *J. Intell. Mater. Syst. Struct.* **2016**, *27*, 314.
- [34] H. Lu, X. Wang, K. Yu, W. M. Huang, Y. Yao, J. Leng, *Smart Mater. Struct.* **2017**, *26*, 095011.
- [35] H. Lu, X. Wang, Y. Yao, Y. Q. Fu, *Smart Mater. Struct.* **2018**, *27*, 065023.
- [36] C. M. Yakacki, R. Shandas, D. Safranski, A. M. Ortega, K. Sassaman, K. Gall, *Adv. Funct. Mater.* **2008**, *18*, 2428.
- [37] J. H. Yang, B. C. Chun, Y.-C. Chung, J. H. Cho, *Polymer* **2003**, *44*, 3251.
- [38] H. M. Jeong, S. Y. Lee, B. K. Kim, *J. Mater. Sci.* **2000**, *35*, 1579.
- [39] A. L. Sisson, D. Ekinici, A. Lendlein, *Polymer* **2013**, *54*, 4333.
- [40] A. Lendlein, H. Jiang, O. Jünger, R. Langer, *Nature* **2005**, *434*, 879.
- [41] L. Wu, C. Jin, X. Sun, *Biomacromolecules* **2011**, *12*, 235.
- [42] J. M. Rochette, V. S. Ashby, *Macromolecules* **2013**, *46*, 2134.
- [43] S.-Q. Wang, D. Kaneko, M. Okajima, K. Yasaki, S. Tateyama, T. Kaneko, *Angew. Chem., Int. Ed.* **2013**, *52*, 11143.
- [44] Y. Gu, Z. Zhao, D. Chao, X. Liu, *Macromol. Res.* **2019**.
- [45] K. M. Lee, N. V. Tabiryan, T. J. Bunning, T. J. White, *J. Mater. Chem.* **2012**, *22*, 691.
- [46] K. M. Lee, D. H. Wang, H. Koerner, R. A. Vaia, L.-S. Tan, T. J. White, *Angew. Chem., Int. Ed.* **2012**, *51*, 4117.
- [47] X. Zhang, C. Zhu, B. Xu, L. Qin, J. Wei, Y. Yu, *ACS Appl. Mater. Interfaces* **2019**, *11*, 46212.
- [48] D. Aoki, Y. Teramoto, Y. Nishio, *Biomacromolecules* **2007**, *8*, 3749.
- [49] J. R. Kumpfer, S. J. Rowan, *J. Am. Chem. Soc.* **2011**, *133*, 12866.
- [50] B. T. Michal, C. A. Jaye, E. J. Spencer, S. J. Rowan, *ACS Macro Lett.* **2013**, *2*, 694.
- [51] K. Yu, Q. Shi, M. L. Dunn, T. Wang, H. J. Qi, *Adv. Funct. Mater.* **2016**, *26*, 6098.
- [52] D. Montarnal, M. Capelot, F. Tournilhac, L. Leibler, *Science* **2011**, *334*, 965.

- [53] K. K. Westbrook, P. H. Kao, F. Castro, Y. Ding, H. Jerry Qi, *Mech. Mater.* **2011**, *43*, 853.
- [54] H. Koerner, G. Price, N. A. Pearce, M. Alexander, R. A. Vaia, *Nat. Mater.* **2004**, *3*, 115.
- [55] M. Behl, K. Kratz, J. Zotzmann, U. Nöchel, A. Lendlein, *Adv. Mater.* **2013**, *25*, 4466.
- [56] L. F. Fan, M. Z. Rong, M. Q. Zhang, X. D. Chen, *J. Mater. Chem. A* **2018**, *6*, 16053.
- [57] Y. Meng, J. Jiang, M. Anthamatten, *ACS Macro Lett.* **2015**, *4*, 115.
- [58] Y. Gao, W. Liu, S. Zhu, *Ind. Eng. Chem. Res.* **2019**, *58*, 19495.
- [59] J. Zhou, S. A. Turner, S. M. Brosnan, Q. Li, J.-M. Y. Carrillo, D. Nykpanchuk, O. Gang, V. S. Ashby, A. V. Dobrynin, S. S. Sheiko, *Macromolecules* **2014**, *47*, 1768.
- [60] B. J. Jin, H. J. Song, R. Q. Jiang, J. Z. Song, Q. Zhao, T. Xie, *Sci. Adv.* **2018**, *4*, 6.
- [61] H. Li, X. Liang, W. Song, *Acta Mech. Sin.* **2019**, *35*, 1217.
- [62] H. Finkelmann, H.-J. Kock, G. Rehage, *Makromol. Chem., Rapid Commun.* **1981**, *2*, 317.
- [63] M. Rogóż, H. Zeng, C. Xuan, D. S. Wiersma, P. Wasylczyk, *Adv. Opt. Mater.* **2016**, *4*, 1689.
- [64] T. H. Ware, M. E. McConney, J. J. Wie, V. P. Tondiglia, T. J. White, *Science* **2015**, *347*, 982.
- [65] T. H. Ware, J. S. Biggins, A. F. Shick, M. Warner, T. J. White, *Nat. Commun.* **2016**, *7*, 10781.
- [66] C. M. Yakacki, M. Saed, D. P. Nair, T. Gong, S. M. Reed, C. N. Bowman, *RSC Adv.* **2015**, *5*, 18997.
- [67] Z. Wang, H. Tian, Q. He, S. Cai, *ACS Appl. Mater. Interfaces* **2017**, *9*, 33119.
- [68] M. O. Saed, A. H. Torbati, D. P. Nair, C. M. Yakacki, *JoVE* **2016**, e53546.
- [69] Y.-Y. Xiao, Z.-C. Jiang, X. Tong, Y. Zhao, *Adv. Mater.* **2019**, *31*, 1903452.
- [70] K. Yu, T. Xie, J. Leng, Y. Ding, H. J. Qi, *Soft Matter* **2012**, *8*, 5687.
- [71] I. Bellin, S. Kelch, R. Langer, A. Lendlein, *Proc. Natl. Acad. Sci. USA* **2006**, *103*, 18043.
- [72] U. N. Kumar, K. Kratz, M. Behl, A. Lendlein, *eXPRESS Polym. Lett.* **2012**, *6*, 26.
- [73] J. Zotzmann, M. Behl, D. Hofmann, A. Lendlein, *Adv. Mater.* **2010**, *22*, 3424.
- [74] S. Chen, J. Hu, C.-W. Yuen, L. Chan, H. Zhuo, *Polym. Adv. Technol.* **2010**, *21*, 377.
- [75] Y. Niu, P. Zhang, J. Zhang, L. Xiao, K. Yang, Y. Wang, *Polym. Chem.* **2012**, *3*, 2508.
- [76] J. Zhang, Y. Niu, C. Huang, L. Xiao, Z. Chen, K. Yang, Y. Wang, *Polym. Chem.* **2012**, *3*, 1390.
- [77] L. Wang, X. Yang, H. Chen, T. Gong, W. Li, G. Yang, S. Zhou, *ACS Appl. Mater. Interfaces* **2013**, *5*, 10520.
- [78] J. Zotzmann, M. Behl, Y. Feng, A. Lendlein, *Adv. Funct. Mater.* **2010**, *20*, 3583.
- [79] M. Behl, I. Bellin, S. Kelch, W. Wagermaier, A. Lendlein, *Adv. Funct. Mater.* **2009**, *19*, 102.
- [80] J. Zotzmann, M. Behl, A. Lendlein, *Macromol. Symp.* **2011**, *309–310*, 147.
- [81] H. Qin, P. T. Mather, *Macromolecules* **2009**, *42*, 273.
- [82] M.-q. Li, F. Song, L. Chen, X.-l. Wang, Y.-z. Wang, *ACS Sustainable Chem. Eng.* **2016**, *4*, 3820.
- [83] S.-k. Ahn, P. Deshmukh, R. M. Kasi, *Macromolecules* **2010**, *43*, 7330.
- [84] S.-k. Ahn, R. M. Kasi, *Adv. Funct. Mater.* **2011**, *21*, 4543.
- [85] L. Xiao, M. Wei, M. Zhan, J. Zhang, H. Xie, X. Deng, K. Yang, Y. Wang, *Polym. Chem.* **2014**, *5*, 2231.
- [86] X. Luo, P. T. Mather, *Adv. Funct. Mater.* **2010**, *20*, 2649.
- [87] R. Hoeher, T. Raidt, C. Krumm, M. Meuris, F. Katzenberg, J. C. Tiller, *Macromol. Chem. Phys.* **2013**, *214*, 2725.
- [88] H. Chen, Y. Liu, T. Gong, L. Wang, K. Zhao, S. Zhou, *RSC Adv.* **2013**, *3*, 7048.
- [89] S. Chen, H. Yuan, Z. Ge, S. Chen, H. Zhuo, J. Liu, *J. Mater. Chem. C* **2014**, *2*, 1041.
- [90] K. Yang, J. Du, Z. Zhang, T. Ren, *Mater. Lett.* **2019**, *257*, 126753.
- [91] T. Xie, *Nature* **2010**, *464*, 267.
- [92] Y. Luo, Y. Guo, X. Gao, B.-G. Li, T. Xie, *Adv. Mater.* **2013**, *25*, 743.
- [93] J. Li, T. Liu, S. Xia, Y. Pan, Z. Zheng, X. Ding, Y. Peng, *J. Mater. Chem.* **2011**, *21*, 12213.
- [94] L. Wang, X. Yang, H. Chen, G. Yang, T. Gong, W. Li, S. Zhou, *Polym. Chem.* **2013**, *4*, 4461.
- [95] T. Xie, *Polymer* **2011**, *52*, 4985.
- [96] Y. Bai, C. Jiang, Q. Wang, T. Wang, *Macromol. Chem. Phys.* **2013**, *214*, 2465.
- [97] R. Dolog, R. A. Weiss, *Macromolecules* **2013**, *46*, 7845.
- [98] H. Luo, J. Hu, Y. Zhu, *Macromol. Chem. Phys.* **2011**, *212*, 1981.
- [99] T. Bai, Y. Han, P. Zhang, W. Wang, W. Liu, *Soft Matter* **2012**, *8*, 6846.
- [100] B. Han, Y.-L. Zhang, Q.-D. Chen, H.-B. Sun, *Adv. Funct. Mater.* **2018**, *28*, 1802235.
- [101] H. Lu, Y. Liu, J. Gou, J. Leng, S. Du, *Compos. Sci. Technol.* **2011**, *71*, 1427.
- [102] J. S. Leng, W. M. Huang, X. Lan, Y. J. Liu, S. Y. Du, *Appl. Phys. Lett.* **2008**, *92*, 204101.
- [103] F. Zhang, Y. Xia, L. Wang, L. Liu, Y. Liu, J. Leng, *ACS Appl. Mater. Interfaces* **2018**, *10*, 35526.
- [104] J. W. Cho, J. W. Kim, Y. C. Jung, N. S. Goo, *Macromol. Rapid Commun.* **2005**, *26*, 412.
- [105] I. H. Paik, N. S. Goo, Y. C. Jung, J. W. Cho, *Smart Mater. Struct.* **2006**, *15*, 1476.
- [106] X. Wan, F. Zhang, Y. Liu, J. Leng, *Carbon* **2019**, *155*, 77.
- [107] H. Lv, J. Leng, S. Du, in *Proc. 15th Int. Symp. Smart Structure Materials*, SPIE, San Diego, CA **2008**.
- [108] L. Lin, Q. Zhou, M. Li, *Mater. Lett.* **2019**, *256*, 126574.
- [109] C. Qian, Y. Zhu, Y. Dong, Y. Fu, *J. Intell. Mater. Syst. Struct.* **2017**, *28*, 2749.
- [110] J. T. Kim, H. J. Jeong, H. C. Park, H. M. Jeong, S. Y. Bae, B. K. Kim, *React. Funct. Polym.* **2015**, *88*, 1.
- [111] M. Sabzi, L. Jiang, F. Liu, I. Ghasemi, M. Atai, *J. Mater. Chem. A* **2013**, *1*, 8253.
- [112] P. Wang, S. Liu, S. Chen, H. Liu, Y. Wu, L. Liu, *Mater. Lett.* **2018**, *220*, 297.
- [113] H. Luo, *Pigm. Resin Technol.* **2018**, *47*, 1.
- [114] N. G. Sahoo, Y. C. Jung, N. S. Goo, J. W. Cho, *Macromol. Mater. Eng.* **2005**, *290*, 1049.
- [115] F. H. Zhang, Z. C. Zhang, C. J. Luo, I. T. Lin, Y. Liu, J. Leng, S. K. Smoukov, *J. Mater. Chem. C* **2015**, *3*, 11290.
- [116] T. Gong, W. Li, H. Chen, L. Wang, S. Shao, S. Zhou, *Acta Biomater.* **2012**, *8*, 1248.
- [117] Q. Ze, X. Kuang, S. Wu, J. Wong, S. M. Montgomery, R. Zhang, J. M. Kovitz, F. Yang, H. J. Qi, R. Zhao, *Adv. Mater.* **2020**, *32*, 1906657.
- [118] P. Testa, R. W. Style, J. Cui, C. Donnelly, E. Borisova, P. M. Derlet, E. R. Dufresne, L. J. Heyderman, *Adv. Mater.* **2019**, *31*, 1900561.
- [119] H. Zhang, Y. Zhao, *ACS Appl. Mater. Interfaces* **2013**, *5*, 13069.
- [120] Q. Guo, C. J. Bishop, R. A. Meyer, D. R. Wilson, L. Olasov, D. E. Schlesinger, P. T. Mather, J. B. Spicer, J. H. Elisseeff, J. J. Green, *ACS Appl. Mater. Interfaces* **2018**, *10*, 13333.
- [121] H. Zhang, J. Zhang, X. Tong, D. Ma, Y. Zhao, *Macromol. Rapid Commun.* **2013**, *34*, 1575.
- [122] R. Tonndorf, M. Kirsten, R.-D. Hund, C. Cherif, *Text. Res. J.* **2015**, *85*, 1305.
- [123] L. Fang, S. Chen, T. Fang, J. Fang, C. Lu, Z. Xu, *Compos. Sci. Technol.* **2017**, *138*, 106.
- [124] A. Toncheva, F. Khelifa, Y. Paint, M. Voué, P. Lambert, P. Dubois, J.-M. Raquez, *ACS Appl. Mater. Interfaces* **2018**, *10*, 29933.
- [125] S. Wu, W. Li, W. Zhou, Y. Zhan, C. Hu, J. Zhuang, H. Zhang, X. Zhang, B. Lei, Y. Liu, *Adv. Opt. Mater.* **2018**, *6*, 1701150.

- [126] W. Wang, D. Shen, X. Li, Y. Yao, J. Lin, A. Wang, J. Yu, Z. L. Wang, S. W. Hong, Z. Lin, S. Lin, *Angew. Chem., Int. Ed.* **2018**, *57*, 2139.
- [127] K. Yu, Y. Liu, J. Leng, *RSC Adv.* **2014**, *4*, 2961.
- [128] H. Kalita, N. Karak, *J. Mater. Res.* **2013**, *28*, 2132.
- [129] W. M. Huang, B. Yang, L. An, C. Li, Y. S. Chan, *Appl. Phys. Lett.* **2005**, *86*, 114105.
- [130] J. Mendez, P. K. Annamalai, S. J. Eichhorn, R. Rusli, S. J. Rowan, E. J. Foster, C. Weder, *Macromolecules* **2011**, *44*, 6827.
- [131] H. Du, J. Zhang, *Soft Matter* **2010**, *6*, 3370.
- [132] F. Zhang, L. Xiong, Y. Ai, Z. Liang, Q. Liang, *Adv. Sci.* **2018**, *5*, 1800450.
- [133] C. Wang, M. Wang, S. Ying, J. Gu, *Macromol. Mater. Eng.* **2020**, *305*, 1900602.
- [134] W. Wang, H. Lu, Y. Liu, J. Leng, *J. Mater. Chem. A* **2014**, *2*, 5441.
- [135] X.-J. Han, Z.-Q. Dong, M.-M. Fan, Y. Liu, J.-H. Li, Y.-F. Wang, Q.-J. Yuan, B.-J. Li, S. Zhang, *Macromol. Rapid Commun.* **2012**, *33*, 1055.
- [136] Y. Li, H. Chen, D. Liu, W. Wang, Y. Liu, S. Zhou, *ACS Appl. Mater. Interfaces* **2015**, *7*, 12988.
- [137] H. Chen, Y. Li, Y. Liu, T. Gong, L. Wang, S. Zhou, *Polym. Chem.* **2014**, *5*, 5168.
- [138] L. R. Khoury, I. Popa, *Nat. Commun.* **2019**, *10*, 5439.
- [139] F. Li, Y. Liu, J. Leng, *Smart Mater. Struct.* **2019**, *28*, 103003.
- [140] T. Chen, O. R. Bilal, R. Lang, C. Daraio, K. Shea, *Phys. Rev. Appl.* **2019**, *11*, 064069.
- [141] V. L. Le, V. T. Le, N. S. Goo, *J. Intell. Mater. Syst. Struct.* **2019**, *30*, 2625.
- [142] S. C. Arzberger, M. L. Tupper, M. S. Lake, R. Barrett, K. Mallick, C. Hazelton, W. Francis, P. N. Keller, D. Campbell, S. Feucht, D. Codell, J. Wintergerst, L. Adams, J. Mallioux, R. Denis, K. White, M. Long, N. A. Munshi, K. Gall, in *Proc. 15th Int. Symp. Smart Structure Materials*, SPIE, San Diego, CA **2005**.
- [143] X. Lan, Y. Liu, H. Lv, X. Wang, J. Leng, S. Du, *Smart Mater. Struct.* **2009**, *18*, 024002.
- [144] Z. Liu, Q. Li, W. Bian, X. Lan, Y. Liu, J. Leng, *Compos. Struct.* **2019**, *223*, 110936.
- [145] R. Zhang, X. Guo, Y. Liu, J. Leng, *Compos. Struct.* **2014**, *112*, 226.
- [146] F. Li, L. Liu, X. Lan, T. Wang, X. Li, F. Chen, W. Bian, Y. Liu, J. Leng, *Int. J. Appl. Mech.* **2016**, *08*, 1640009.
- [147] H. M. C. M. Herath, J. A. Epaarachchi, M. M. Islam, W. Al-Azzawi, J. Leng, F. Zhang, *Compos. Sci. Technol.* **2018**, *167*, 206.
- [148] T. Liu, L. Liu, M. Yu, Q. Li, C. Zeng, X. Lan, Y. Liu, J. Leng, *Compos. Struct.* **2018**, *206*, 164.
- [149] H. Wei, L. Liu, Z. Zhang, H. Du, Y. Liu, J. Leng, *Compos. Struct.* **2015**, *133*, 642.
- [150] F. Li, L. Liu, X. Lan, X. Zhou, W. Bian, Y. Liu, J. Leng, *Int. J. Smart Nano Mater.* **2016**, *7*, 106.
- [151] D. Zhang, L. Liu, J. Leng, Y. Liu, *Compos. Struct.* **2020**, *232*, 111561.
- [152] L. Santo, F. Quadrini, P. L. Ganga, V. Zolesi, *Aerosp. Sci. Technol.* **2015**, *40*, 109.
- [153] F. Li, L. Liu, X. Lan, C. Pan, Y. Liu, J. Leng, Q. Xie, *Smart Mater. Struct.* **2019**, *28*, 075023.
- [154] G. P. Tandon, K. Goecke, K. Cable, J. Baur, *J. Intell. Mater. Syst. Struct.* **2010**, *21*, 1365.
- [155] Q. Tan, F. Li, L. Liu, Y. Liu, X. Yan, J. Leng, *J. Intell. Mater. Syst. Struct.* **2019**, *30*, 2688.
- [156] J. H. Jang, S. B. Hong, J.-G. Kim, N. S. Goo, H. Lee, W.-R. Yu, *Smart Mater. Struct.* **2019**, *28*, 115013.
- [157] Q. Tan, F. Li, L. Liu, H. Chu, Y. Liu, J. Leng, *J. Intell. Mater. Syst. Struct.* **2018**, *29*, 1081.
- [158] J. Sun, Q. Guan, Y. Liu, J. Leng, *J. Intell. Mater. Syst. Struct.* **2016**, *27*, 2289.
- [159] J. Leng, *Aircr. Eng. Aerospace Tech.* **2015**, *87*, 218.
- [160] M. Keihl, R. Bortolin, B. Sanders, S. Joshi, Z. Tidwell, presented at SPIE, San Diego, CA **2005**.
- [161] P. Li, Z. Yan, L. Zhang, Y. Liu, J. Leng, K. T. Lau, *J. Intell. Mater. Syst. Struct.* **2014**, *25*, 1224.
- [162] J. Sun, Y. Liu, J. Leng, *J. Intell. Mater. Syst. Struct.* **2015**, *26*, 2020.
- [163] D. Zhang, O. J. George, K. M. Petersen, A. C. Jimenez-Vergara, M. S. Hahn, M. A. Grunlan, *Acta Biomater.* **2014**, *10*, 4597.
- [164] A. Lendlein, R. Langer, *Science* **2002**, *296*, 1673.
- [165] J. Ortega, D. Maitland, T. Wilson, W. Tsai, Ö. Savaş, D. Saloner, *Ann. Biomed. Eng.* **2007**, *35*, 1870.
- [166] S. M. Herting, Y. Ding, A. J. Boyle, D. Dai, L. D. Nash, S. Asnafi, D. R. Jakaitis, C. R. Johnson, L. M. Graul, C. Yeh, D. F. Kallmes, R. Kadirvel, D. J. Maitland, *J. Biomed. Mater. Res., Part B* **2019**, *107*, 2466.
- [167] M. F. Metzger, T. S. Wilson, D. Schumann, D. L. Matthews, D. J. Maitland, *Biomed. Microdevices* **2002**, *4*, 89.
- [168] D. J. Maitland, T. Wilson, M. Metzger, D. L. Schumann, presented at SPIE, San Diego, CA **2002**.
- [169] J. M. Ortega, W. Small, T. S. Wilson, W. J. Benett, J. M. Loge, D. J. Maitland, *IEEE Trans. Biomed. Eng.* **2007**, *54*, 1722.
- [170] A. Melocchi, M. Uboldi, N. Inverardi, F. Briatico-Vangosa, F. Baldi, S. Pandini, G. Scalet, F. Auricchio, M. Cerea, A. Foppoli, A. Maroni, L. Zema, A. Gazzaniga, *Int. J. Pharm.* **2019**, *571*, 118700.
- [171] C. Lin, J. Lv, Y. Li, F. Zhang, J. Li, Y. Liu, L. Liu, J. Leng, *Adv. Funct. Mater.* **2019**, *29*, 1906569.
- [172] H. M. Wache, D. J. Tartakowska, A. Hentrich, M. H. Wagner, *J. Mater. Sci.: Mater. Med.* **2003**, *14*, 109.
- [173] Y. C. Shin, J. B. Lee, D.-H. Kim, T. Kim, G. Alexander, Y. M. Shin, J. Y. Park, S. Baek, J.-K. Yoon, Y. J. Lee, G. M. Seon, M. H. Lee, M.-L. Kang, W. S. Jang, J.-C. Park, H.-W. Jun, Y. Kim, H.-J. Sung, *Adv. Mater.* **2019**, *31*, 1904476.
- [174] P. R. Buckley, G. H. McKinley, T. S. Wilson, W. Small, W. J. Benett, J. P. Beringer, M. W. Mcelfresh, D. J. Maitland, *IEEE Trans. Biomed. Eng.* **2006**, *53*, 2075.
- [175] K. Yamagishi, A. Nojiri, E. Iwase, M. Hashimoto, *ACS Appl. Mater. Interfaces* **2019**, *11*, 41770.
- [176] M. Musiał-Kulik, J. Kasperczyk, A. Smola, P. Dobrzyński, *Int. J. Pharm.* **2014**, *465*, 291.
- [177] C. Wischke, A. T. Neffe, S. Steuer, A. Lendlein, *J. Controlled Release* **2009**, *138*, 243.
- [178] M. C. Serrano, L. Carbajal, G. A. Ameer, *Adv. Mater.* **2011**, *23*, 2211.
- [179] K. Nagahama, Y. Ueda, T. Ouchi, Y. Ohya, *Biomacromolecules* **2009**, *10*, 1789.
- [180] A. T. Neffe, B. D. Hanh, S. Steuer, A. Lendlein, *Adv. Mater.* **2009**, *21*, 3394.
- [181] M. A. Zainal, A. Ahmad, M. S. Mohamed Ali, *Biomed. Microdevices* **2017**, *19*, 8.
- [182] Z. Yu, Q. Zhang, L. Li, Q. Chen, X. Niu, J. Liu, Q. Pei, *Adv. Mater.* **2011**, *23*, 664.
- [183] Z. Yu, X. Niu, Z. Liu, Q. Pei, *Adv. Mater.* **2011**, *23*, 3989.
- [184] U. Adiyani, T. Larsen, J. J. Zárate, L. G. Villanueva, H. Shea, *Nat. Commun.* **2019**, *10*, 4518.
- [185] J. Wang, Q. Zhao, Y. Wang, Q. Zeng, T. Wu, X. Du, *Adv. Mater. Technol.* **2019**, *4*, 1900566.
- [186] R. Liu, X. Kuang, J. Deng, Y.-C. Wang, A. C. Wang, W. Ding, Y.-C. Lai, J. Chen, P. Wang, Z. Lin, H. J. Qi, B. Sun, Z. L. Wang, *Adv. Mater.* **2018**, *30*, 1705195.
- [187] T. Ware, D. Simon, C. Liu, T. Musa, S. Vasudevan, A. Sloan, E. W. Keefer, R. L. Rennaker II, W. Voit, *J. Biomed. Mater. Res., Part B* **2014**, *102*, 1.
- [188] J. Reeder, M. Kaltenbrunner, T. Ware, D. Arreaga-Salas, A. Avendano-Bolivar, T. Yokota, Y. Inoue, M. Sekino, W. Voit, T. Sekitani, T. Someya, *Adv. Mater.* **2014**, *26*, 4967.
- [189] T. Ware, D. Simon, K. Hearon, C. Liu, S. Shah, J. Reeder, N. Khodaparast, M. P. Kilgard, D. J. Maitland, R. L. Rennaker, 2nd, W. E. Voit, *Macromol. Mater. Eng.* **2012**, *297*, 1193.

- [190] M. A. Stiller, J. Usoro, L. C. Frewin, R. V. Danda, M. Ecker, A. Joshi-Imre, C. K. Musselman, W. Voit, R. Modi, J. J. Pancrazio, J. B. Black, *Micromachines* **2018**, *9*, 500.
- [191] T. Sekitani, U. Zschieschang, H. Klauk, T. Someya, *Nat. Mater.* **2010**, *9*, 1015.
- [192] Y. Zhang, N. Zheng, Y. Cao, F. Wang, P. Wang, Y. Ma, B. Lu, G. Hou, Z. Fang, Z. Liang, M. Yue, Y. Li, Y. Chen, J. Fu, J. Wu, T. Xie, X. Feng, *Sci. Adv.* **2019**, *5*, eaaw1066.
- [193] T. Pretschi, M. Ecker, M. Schildhauer, M. Maskos, *J. Mater. Chem.* **2012**, *22*, 7757.
- [194] W. Li, Y. Liu, J. Leng, *ACS Appl. Mater. Interfaces* **2017**, *9*, 44792.
- [195] G. Zhang, W. Peng, J. Wu, Q. Zhao, T. Xie, *Nat. Commun.* **2018**, *9*, 4002.
- [196] M. Yamada, M. Kondo, R. Miyasato, Y. Naka, J.-i. Mamiya, M. Kinoshita, A. Shishido, Y. Yu, C. J. Barrett, T. Ikeda, *J. Mater. Chem.* **2009**, *19*, 60.
- [197] C. Wang, K. Sim, J. Chen, H. Kim, Z. Rao, Y. Li, W. Chen, J. Song, R. Verduzco, C. Yu, *Adv. Mater.* **2018**, *30*, 1706695.
- [198] Z. Xu, C. Ding, D.-W. Wei, R.-Y. Bao, K. Ke, Z. Liu, M.-B. Yang, W. Yang, *ACS Appl. Mater. Interfaces* **2019**, *11*, 30332.
- [199] Q. Yang, C. Peng, J. Ren, W. Zhao, W. Zheng, C. Zhang, Y. Hu, X. Zhang, *Adv. Opt. Mater.* **2019**, *7*, 1900784.
- [200] H. Wei, X. Cauchy, I. O. Navas, Y. Abderrafai, K. Chizari, U. Sundararaj, Y. Liu, J. Leng, D. Therriault, *ACS Appl. Mater. Interfaces* **2019**, *11*, 24523.
- [201] Y.-F. Zhang, N. Zhang, H. Hingorani, N. Ding, D. Wang, C. Yuan, B. Zhang, G. Gu, Q. Ge, *Adv. Funct. Mater.* **2019**, *29*, 1806698.
- [202] Q. Ge, A. H. Sakhaei, H. Lee, C. K. Dunn, N. X. Fang, M. L. Dunn, *Sci. Rep.* **2016**, *6*, 31110.
- [203] D. McCoul, S. Rosset, N. Besse, H. Shea, *Smart Mater. Struct.* **2017**, *26*, 025015.
- [204] J. A. C. Liu, J. H. Gillen, S. R. Mishra, B. A. Evans, J. B. Tracy, *Sci. Adv.* **2019**, *5*, eaaw2897.
- [205] Q. He, Z. Wang, Y. Wang, A. Minori, M. T. Tolley, S. Cai, *Sci. Adv.* **2019**, *5*, 7.
- [206] T. Chen, K. Shea, *3D Print. Addit. Manuf.* **2018**, *5*, 91.
- [207] T. Chen, O. R. Bilal, K. Shea, C. Daraio, *Proc. Natl. Acad. Sci. USA* **2018**, *115*, 5698.
- [208] Y. Zhang, Y. Li, Y. Hu, X. Zhu, Y. Huang, Z. Zhang, S. Rao, Z. Hu, W. Qiu, Y. Wang, G. Li, L. Yang, J. Li, D. Wu, W. Huang, C. Qiu, J. Chu, *Adv. Mater.* **2018**, *30*, 1803072.
- [209] C.-M. Chen, S. Yang, *Adv. Mater.* **2014**, *26*, 1283.
- [210] C.-M. Chen, C.-L. Chiang, S. Yang, *Langmuir* **2015**, *31*, 9523.
- [211] Z. Cheng, D. Zhang, T. Lv, H. Lai, E. Zhang, H. Kang, Y. Wang, P. Liu, Y. Liu, Y. Du, S. Dou, L. Jiang, *Adv. Funct. Mater.* **2018**, *28*, 1705002.
- [212] T. Lv, Z. Cheng, D. Zhang, E. Zhang, Q. Zhao, Y. Liu, L. Jiang, *ACS Nano* **2016**, *10*, 9379.
- [213] C.-C. Fu, A. Grimes, M. Long, C. G. L. Ferri, B. D. Rich, S. Ghosh, S. Ghosh, L. P. Lee, A. Gopinathan, M. Khine, *Adv. Mater.* **2009**, *21*, 4472.
- [214] Y. Zhao, W. M. Huang, Y. Q. Fu, *J. Micromech. Microeng.* **2011**, *21*, 067007.
- [215] M. Ebara, K. Uto, N. Idota, J. M. Hoffman, T. Aoyagi, *Adv. Mater.* **2012**, *24*, 273.
- [216] J. Yang, W. Zhao, Z. Yang, W. He, J. Wang, T. Ikeda, L. Jiang, *ACS Appl. Mater. Interfaces* **2019**, *11*, 46124.
- [217] S. G. Romanov, G. Lozano, D. Gerace, C. Monat, H. R. Míguez, A. Espinha, M. Concepción Serrano, Á. Blanco, C. López, presented at *Photonic Crystal Materials and Devices XI*, Brussels, Belgium **2014**.
- [218] Y. Fang, Y. Ni, S. Y. Leo, B. Wang, V. Basile, C. Taylor, P. Jiang, *ACS Appl. Mater. Interfaces* **2015**, *7*, 23650.
- [219] P. Wu, X. Shen, C. G. Schäfer, J. Pan, J. Guo, C. Wang, *Nanoscale* **2019**, *11*, 20015.
- [220] Y. Xie, Y. Meng, W. Wang, E. Zhang, J. Leng, Q. Pei, *Adv. Funct. Mater.* **2018**, *28*, 1802430.
- [221] S. Tibbitts, *Archit. Des.* **2014**, *84*, 116.
- [222] A. Sydney Gladman, E. A. Matsumoto, R. G. Nuzzo, L. Mahadevan, J. A. Lewis, *Nat. Mater.* **2016**, *15*, 413.
- [223] Y. Mao, Z. Ding, C. Yuan, S. Ai, M. Isakov, J. Wu, T. Wang, M. L. Dunn, H. J. Qi, *Sci. Rep.* **2016**, *6*, 24761.
- [224] W. Zhang, F. Zhang, X. Lan, J. Leng, A. S. Wu, T. M. Bryson, C. Cotton, B. Gu, B. Sun, T.-W. Chou, *Compos. Sci. Technol.* **2018**, *160*, 224.
- [225] H. Wei, Q. Zhang, Y. Yao, L. Liu, Y. Liu, J. Leng, *ACS Appl. Mater. Interfaces* **2017**, *9*, 876.
- [226] L. Huang, R. Jiang, J. Wu, J. Song, H. Bai, B. Li, Q. Zhao, T. Xie, *Adv. Mater.* **2017**, *29*, 1605390.
- [227] Y. Zhang, L. Huang, H. Song, C. Ni, J. Wu, Q. Zhao, T. Xie, *ACS Appl. Mater. Interfaces* **2019**, *11*, 32408.
- [228] S. Deng, J. Wu, M. D. Dickey, Q. Zhao, T. Xie, *Adv. Mater.* **2019**, *31*, 1903970.
- [229] S. Miao, W. Zhu, N. J. Castro, M. Nowicki, X. Zhou, H. Cui, J. P. Fisher, L. G. Zhang, *Sci. Rep.* **2016**, *6*, 27226.
- [230] J. Liu, O. Erol, A. Pantula, W. Liu, Z. Jiang, K. Kobayashi, D. Chatterjee, N. Hibino, L. H. Romer, S. H. Kang, T. D. Nguyen, D. H. Gracias, *ACS Appl. Mater. Interfaces* **2019**, *11*, 8492.
- [231] F. S. Senatov, M. Y. Zadorozhnyy, K. V. Niaza, V. V. Medvedev, S. D. Kaloshkin, N. Y. Anisimova, M. V. Kiselevskiy, K.-C. Yang, *Eur. Polym. J.* **2017**, *93*, 222.
- [232] F. Zhang, L. Wang, Z. Zheng, Y. Liu, J. Leng, *Composites, Part A* **2019**, *125*, 105571.
- [233] W. Zhao, F. Zhang, J. Leng, Y. Liu, *Compos. Sci. Technol.* **2019**, *184*, 107866.
- [234] S. Kim, M. Sitti, T. Xie, X. Xiao, *Soft Matter* **2009**, *5*, 3689.
- [235] J. Eisenhaure, S. Kim, *Int. J. Adhes. Adhes.* **2018**, *81*, 74.
- [236] J. K. Park, J. D. Eisenhaure, S. Kim, *Adv. Mater. Interfaces* **2019**, *6*, 1801542.
- [237] J. Seo, J. Eisenhaure, S. Kim, *Extreme Mech. Lett.* **2016**, *9*, 207.
- [238] J. Eisenhaure, S. Kim, *Polymers* **2014**, *6*, 2274.
- [239] T. Xie, X. Xiao, *Chem. Mater.* **2008**, *20*, 2866.
- [240] R. Wang, X. Xiao, T. Xie, *Macromol. Rapid Commun.* **2010**, *31*, 295.
- [241] J. D. Eisenhaure, T. Xie, S. Varghese, S. Kim, *ACS Appl. Mater. Interfaces* **2013**, *5*, 7714.
- [242] D. Tan, X. Wang, Q. Liu, K. Shi, B. Yang, S. Liu, Z.-S. Wu, L. Xue, *Small* **2019**, *15*, 1904248.
- [243] C.-M. Chen, C.-L. Chiang, C.-L. Lai, T. Xie, S. Yang, *Adv. Funct. Mater.* **2013**, *23*, 3813.
- [244] Y. Xue, Y. Zhang, X. Feng, S. Kim, J. A. Rogers, Y. Huang, *J. Mech. Phys. Solids* **2015**, *77*, 27.
- [245] Y. Huang, N. Zheng, Z. Cheng, Y. Chen, B. Lu, T. Xie, X. Feng, *ACS Appl. Mater. Interfaces* **2016**, *8*, 35628.
- [246] J. D. Eisenhaure, S. I. Rhee, A. M. Al-Okaily, A. Carlson, P. M. Ferreira, S. Kim, *J. Microelectromech. Syst.* **2016**, *25*, 69.
- [247] C. Linghu, S. Zhang, C. Wang, K. Yu, C. Li, Y. Zeng, H. Zhu, X. Jin, Z. You, J. Song, *Sci. Adv.* **2020**, *6*, eaay5120.
- [248] G. Li, N. Uppu, *Compos. Sci. Technol.* **2010**, *70*, 1419.
- [249] G. Li, D. Nettles, *Polymer* **2010**, *51*, 755.
- [250] G. Li, H. Meng, J. Hu, *J. R. Soc., Interface* **2012**, *9*, 3279.
- [251] J. Hu, S. Chung, Y. Li, *Trans. Inst. Meas. Control* **2007**, *29*, 301.
- [252] H. Narayana, J. Hu, B. Kumar, S. Shang, J. Han, P. Liu, T. Lin, F. Ji, Y. Zhu, *J. Mater. Chem. B* **2017**, *5*, 1905.
- [253] S. Chen, J. Hu, C.-w. Yuen, L. Chan, *Polymer* **2009**, *50*, 4424.
- [254] J. Chen, J. Hu, A. K. L. Leung, C. Chen, J. Zhang, Y. Zhang, Y. Zhu, J. Han, *ACS Appl. Mater. Interfaces* **2018**, *10*, 32935.